Summer 2017

Dynamic electromechanical characterization of ferroelectrics at cryogenic temperatures

William Kent Hays

Department:

DYNAMIC ELECTROMECHANICAL CHARACTERIZATION OF FERROELECTRICS AT CRYOGENIC TEMPERATURES

by

WILLIAM KENT HAYS

A THESIS

Presented to the Graduate Faculty of the

MISSOURI UNIVERSITY OF SCIENCE AND TECHNOLOGY

In Partial Fulfillment of the Requirements for the Degree

MASTER OF SCIENCE

in

MECHANICAL ENGINEERING

2017

Approved by

Dr. Charles Wojnar, Advisor
Dr. Daniel Stutts
Dr. Lokesh Dharani

ABSTRACT

Electromechanical coupling in ferroelectric materials has given rise to a myriad of technological applications. Through the complex domain structure of ferroelectrics materials, which are typically stiff and have low damping, can exhibit significant structural damping. The applications for a material with a relatively large Young's modulus and the ability to damp out vibrations would be useful for structures, more specifically, aerospace structures. The dynamic mechanical properties of ferroelectrics, particularly mechanical properties while an electric field is applied, are not well understood. This is due in part to the lack of experimental methods to measure such properties. Even with recent advancements in these testing methods, there still exists a gap in the ability to measure the dynamic electromechanical response of ferroelectrics over wide ranges of temperature (in particular at low temperatures for e.g. space applications). To this end, the cryogenic broadband electromechanical spectroscopy (CBES) experimental apparatus was designed and constructed, and a particular ferroelectric material, lead zirconate titanate (PZT) was tested. The CBES is a new experimental set-up allowing for the measurement of dynamic mechanical, electrical and temperature dependent properties of materials within the cryogenic temperature region. The CBES expands the current state of the art testing abilities for ferroelectrics, allowing for the simultaneous application of dynamic electrical and mechanical loads in a space-like environment, with temperatures ranging from 34-325 K. This study will review current testing capabilities and highlight the need to test ferroelectrics in this environment. The capabilities of the novel CBES and results from cryogenic viscoelastic measurements are presented, demonstrating the temperature dependent relationship between electric properties (polarization) and the viscoelastic properties (loss tangent and dynamic Young's modulus) of PZT. The possible future applications for the CBES are also discussed.

ACKNOWLEDGMENTS

I would first like to thank my parents for believing in and supporting me throughout my education and throughout my whole life. You have always been supportive and encouraging with anything I attempted, and for that I will be forever grateful. Secondly I would like to thank my advisor Dr. Charles (Stan) Wojnar, without your guidance, patience and most importantly your willingness to help teach and assist me throughout my research I would not have made it this far. I has been great to work for and with you and it has was a privilege to be your first graduate student. I would also like to thank my committee members Dr. Daniel Stutts, and Dr. Lokesh Dharani, you were always willing to help, I am grateful for your advice throughout my time at Missouri S&T. Lastly I would like to thank my friends and family who have always been there for me.

TABLE OF CONTENTS

Page

LIST OF ILLUSTRATIONS

LIST OF TABLES

1. INTRODUCTION

Physicists, scientists, and engineers continually make progress in the field of material science as new materials, specifically smart materials, (ones with tunable properties), are being discovered and developed. As part of the growing category of smart materials, ferroelectrics, which are the focus of this study, are finding increased use in technological applications. As will be discussed more in depth, ferroelectric materials are a special class of materials that exhibit thermo-electromechanical coupling, which enables their diverse application.

In the development of new materials or devices it is necessary to fully understand the physics that gives rise to their overall properties in order for them to be properly utilized. Physics-based material modeling is important for our understanding of the underlying physics. However, in order to validate such models, experimental data is required, and the complexity of ferroelectric materials necessitate the development of special experimental equipment. To this end, the objective of this study is the construction and validation of an experimental apparatus designed to test the viscoelastic and dielectric properties of bulk ferroelectric ceramic materials through simultaneous thermal, electrical, and mechanical loading. The measured material properties will aid in fundamental understanding of the underlying material physics. In the following sections we introduce ferroelectricity, and then a discuss current applications of ferroelectrics as well as existing methods for their characterization. Lastly the motivation to develop the new testing apparatus for bulk ferroelectric ceramics and an outline for the thesis will be given.

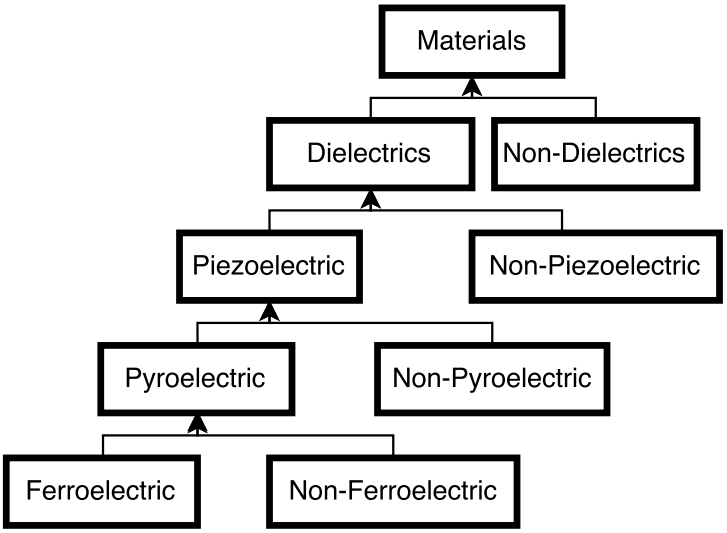

Figure 1.1. Flowchart showing the classification of ferroelectrics.

1.1. INTRODUCTION TO FERROELECTRICS

Ferroelectrics are a sub-class of pyroelectrics, which are themselves a sub-class of piezoelectrics. Piezoelectrics are a sub-class of dielectrics which are a direct class under all materials. The classes and sub-classes are shown in the diagram in Figure 1.1.

Dielectric materials are polarizable, electrically-insulating materials. The dielectric phenomena is what is used in capacitors. The insulating properties allows for a voltage, V, to be applied without a current passing through the material. Instead, the material becomes electrically polarized with polarization, p, which gives rise to the build up of charge, Q, on the specimen's surfaces as shown in Figure 1.2.

Piezoelectrics are dielectric materials that exhibit electromechanical coupling, that is to say when piezoelectrics are subjected to an electric field, they will exhibit a mechanical strain; the inverse is true, when under a mechanical stress a charge is accumulated on the specimen's surface. In the presence of relativity low applied electric fields, piezoelectric materials have a linear relationship between the applied electric field and strain.

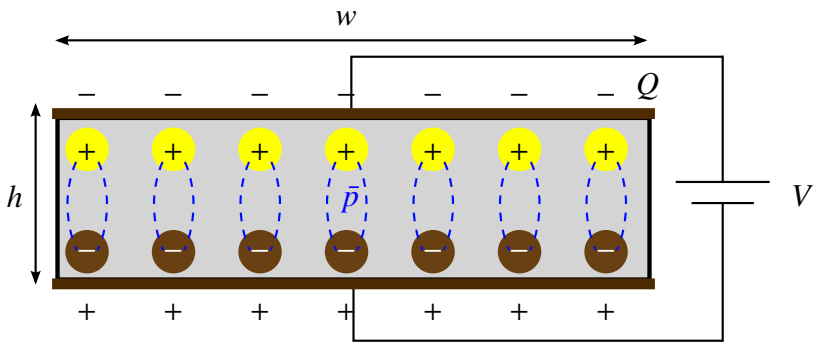

Figure 1.2. Capacitor with internal polarization due to an applied voltage adapted with permission from [74].

Pyroelectrics are piezoelectric materials with two distinct qualifiers, they have a spontaneous polarization, such that when no stress or electric field is applied there is a discernible polarization, and this polarization is dependent on temperature, hence pyro- in the name pyroelectrics (see Figure 1.3).

Lastly the ferroelectric sub-class of materials, which exhibit all of the same properties of pyroelectric materials with the distinction that the spontaneous polarization direction is able to be reoriented. Such that, under a sufficiently large electric field, called the coercive field, the spontaneous or remnant polarization exhibited by all pyroelectric materials is able to be switched. This polarization switching results in a hysteretic effect under cyclic loading, which can be observed in Figure 1.4.

Piezoelectrics have been studied for over a century. Jacques and Pierre Curie studied naturally occurring piezoelectric materials such as quartz, topaz, and Seignette's (Rochelle) salt in the 1880's [15]. Earlier, studies into pyroelectrics, were carried out to understand the phenomena [5, 68]. Valasek was the first person to discover ferroelectricity in 1921 [71]. Despite the *ferro* prefix, most ferroelectrics do not contain iron, instead ferroelectricity is the namesake of ferromagnetism, which was already known at the time Valasek discovered ferroelectricity.

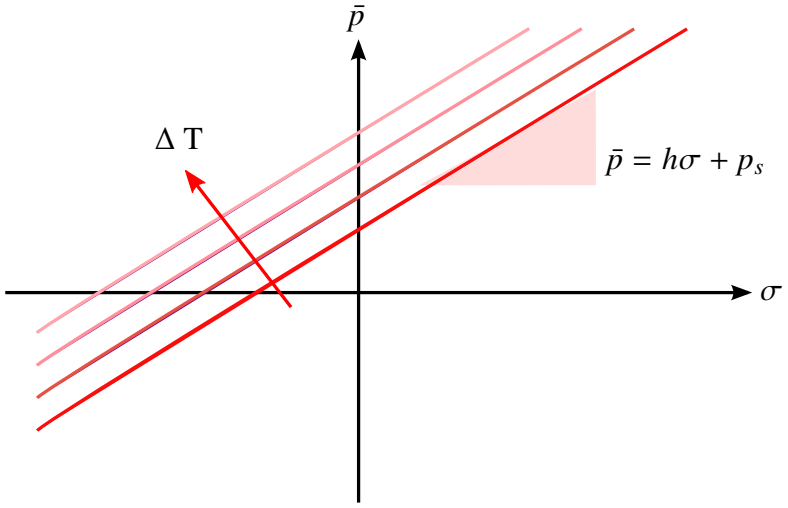

Figure 1.3. Graph of polarization vs stress (under relatively low electric fields) showing the spontaneous polarization. The temperature dependence of pyroelectrics can be observed by the change in the spontaneous polarization vs the change in temperature.

1.2. PHYSICS BEHIND FERROELECTRICITY

Ferroelectrics are a subset of piezoelectrics, hence they exhibit piezoelectricity. Piezoelectricity arises due to electric dipoles in materials. The dipole is induced as a result of asymmetry in the crystal lattice for crystalline materials. In polymers, the electric displacement can be induced by the dipoles found in molecular groups. For brevity only piezoelectricity and ferroelectricity in crystalline ceramics will be discussed in this thesis. To understand the mechanisms behind piezoelectricity and specifically ferroelectricity in polymers one should reference [44]. As shown in Figure 1.5, a simple atomic structure of Si^+ and O^-, which make up quartz, can be repeated in a fashion where the net polarity is neutral in the undeformed configuration. However as a stress is applied, the structure will experience strain that distorts the crystal structure and leads to an electric potential across the material indicated by the positive and negative ends.

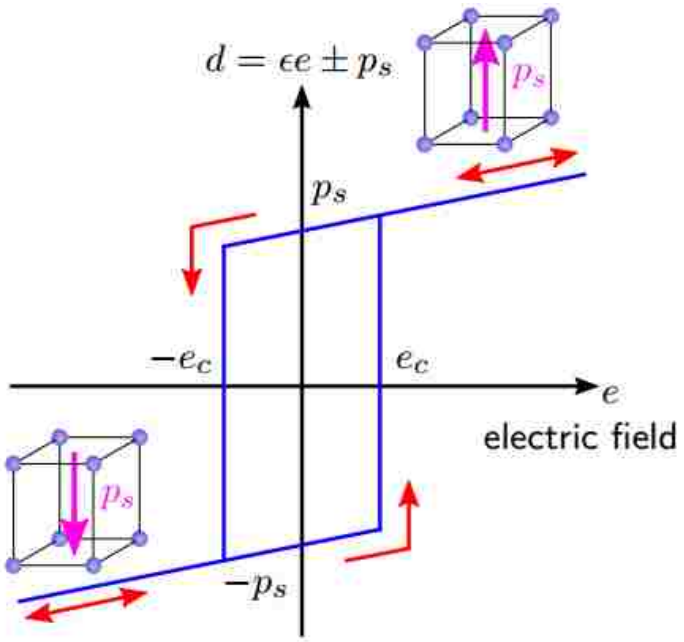

Figure 1.4. Plot of piece-wise linearized version of the electric field versus electric displacement for a ferroelectric material. The characteristic hysteretic curve is observable due to the polarization switching, adapted with permission from [74].

In piezoelectric materials, this electromechanical coupling is linear as shown before in Figure 1.3, such that the polarization versus the stress applied, and conversely the strain versus the charge applied are linearly related at relatively low electric fields. As the stress is removed, the atomic structure returns to its undeformed configuration and the separation between the electric dipoles decreases until returning back to a zero net polarization.

The spontaneous polarization, distinguishing pyroelectrics from piezoelectrics, can be observed in lead zirconate titanate (PZT). The spontaneous polarization occurs only below a material-specific temperature called the Curie temperature. Above this temperature the PZT crystal is cubic. Once the material cools below its Curie temperature, it transitions into a tetragonal crystal. In its tetragonal phase, the center of the unit cell, comprised of Zr^{4+} and Ti^{4+}, is shifted, causing the unit cell to be non-centrosymmetric and leads to an electric dipole. This electric dipole creates a polarization of the material, as shown in Figure

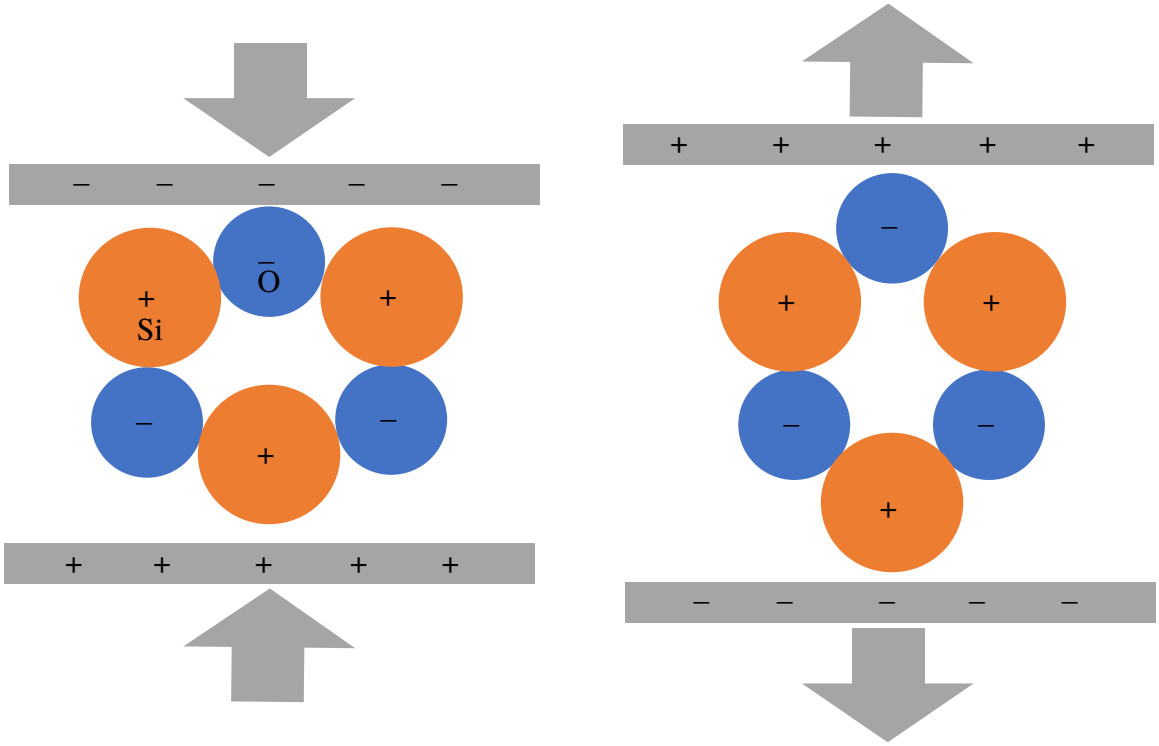

Figure 1.5. Figure showing the piezoelectric effect in quartz; when a stress is applied the crystal deforms and the unbalance of the charges leads to a polarization.

1.6. As the temperature further decreases the electric dipole of the unit cell increases, thus exhibiting the pyroelectric affect. The temperature dependence of polarization in PZT can be modeled as an logarithmic growth in the spontaneous as the material cools from the Curie temperature [37]. This trend can be altered through changing the composition of the material, i.e. manganese doping, can lead to different thermoelectric coupling [64].

The final requirement for a material to be ferroelectric is the ability to reorient or realign the material's electric polarization, referred to as domain switching. This is typically achieved by applying an external electric field that is sufficiently large to force the electric dipole to realign to the favorable position with respect to the external electric field. Recently it has be shown that domain switching can be achieved, in a thin film, by applying a mechanical load [11]. PZT, as mentioned above as a pyroelectric, is also ferroelectric. One can see when looking at the structure of the PZT crystal that the

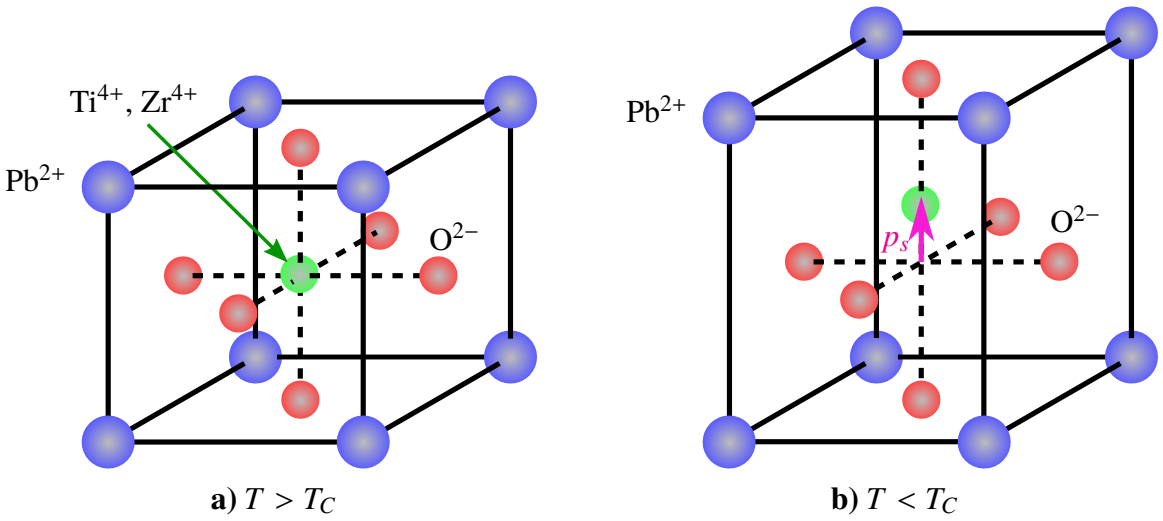

Figure 1.6. As (a) PZT in the cubic phase cools below the curie temperature it transitions to a (b) tetragonal crystal PZT where the spontaneous polarization can be observed adapted with permission from [74].

spontaneous polarization below the Curie temperature moves the Zr^{4+}, or Ti^{4+} nucleus to one of six possible positions all, either 90 or 180 degrees apart. These positions are shown in Figure 1.7. The reorientation of the polarization can be induced by applying the coercive electric field, which will shift the Zr^{4+}, or Ti^{4+} nucleus to one of the six positions that is most favorable with respect to the applied electric field. It should be noted that not all ferroelectrics have the same admissible orientations of polarization. The number of polarization orientations and angle difference between them is dependent on the crystal structure of the particular ferroelectric material.

While it is possible to switch the polarization orientation of a ferroelectric under a coercive field, it should be noted that not all the domains in a bulk specimen switch instantaneously to the coercive field being applied. As an electric field is applied, the favorably oriented domains in a crystal will begin to grow and the less favorable domains will shrink as was shown in Figure 1.8 [24]. This growth and corresponding reduction of domains is called domain wall motion and has been studied and a variety of different models have been developed to capture the underlying physics ([8, 12, 25, 48, 49, 59]). As

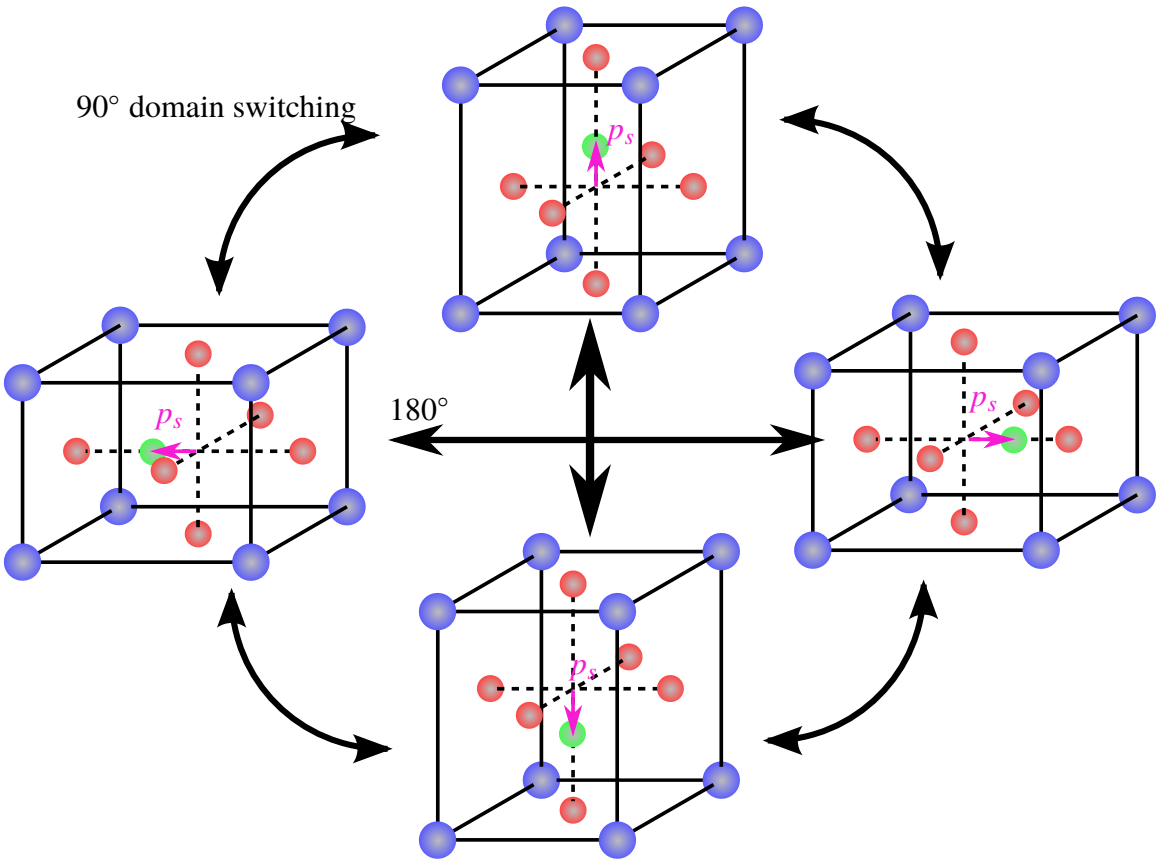

Figure 1.7. Possible spontaneous polarization orientations (with two additional orientations, into and out of the page) in PZT adapted with permission from [74].

the applied electric field tends toward the coercive field, the domain wall velocity increases, and the maximum velocity occurs near the coercive field. This being understood, most experiments and models have looked into domain wall motion below the coercive field, and have determined the velocity of the domain wall motion is a function of the applied electric field, stress, and temperature ([48, 79]). Domain wall motion is significant to this study because the capacity for domain wall motion allows for energy dissipation in a ferroelectrics, which is an important application. Nonetheless few studies have focused on dynamic mechanical properties during domain switching, with none focused on the influence of low temperatures.

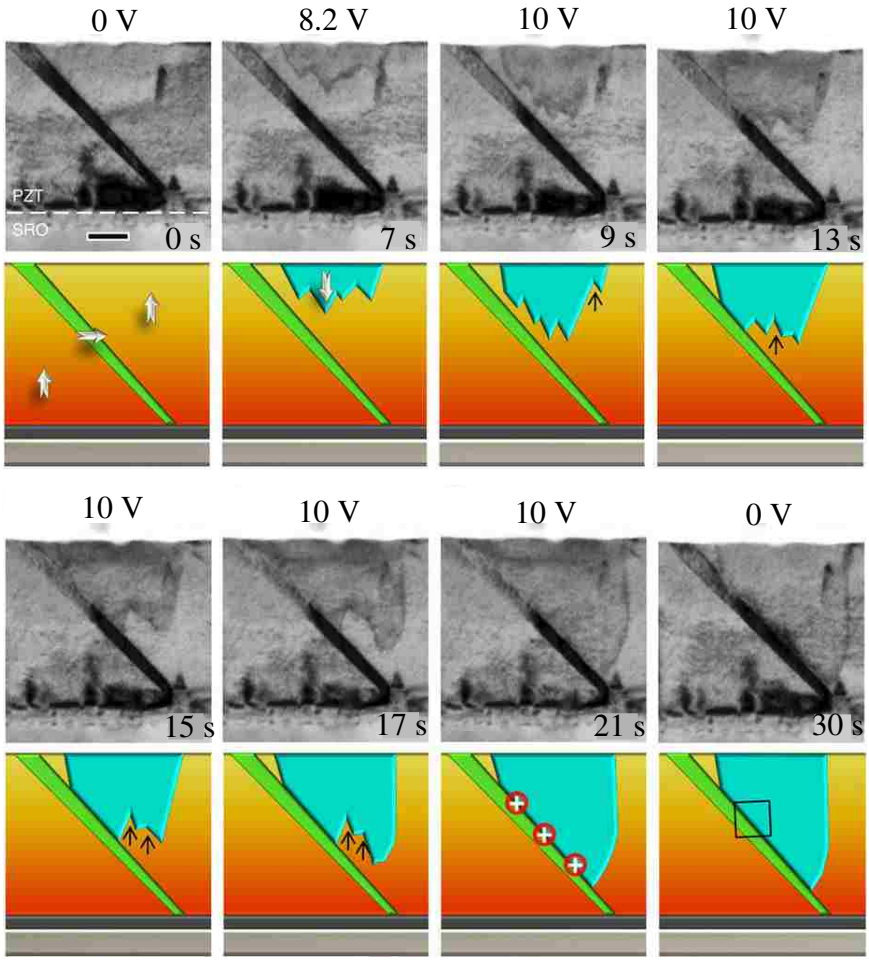

Figure 1.8. Growth of favorable domains under applied electric field [24].

In the next section previous and current applications and experimentation on ferroelectric materials will be discussed, including experiments involving the application of thermal, electrical, and mechanical loads. The goal of this discussion is to highlight the limitations of current experimental methods on studying the influence of temperature, electric fields, and stress on the properties of ferroelectrics. The new capabilities of the apparatus developed will close this gap.

1.3. APPLICATIONS OF PIEZO/PYRO/FERROELECTRICS

Due to the unique electromechanical coupling, thermoelectrical coupling, and polarization orientation and reorientation characteristics of ferroelectrics, they are used in a myriad of technological applications. Common applications of ferroelectrics are sensors and actuators. Sensors typically make use of either the electromechanical and thermoelectric coupling by transforming pressure or temperature gradients, respectively, into measurable electric signals. Actuators take the reverse electromechanical coupling effect and use an electrical input to output a displacement, sometimes using it to create sound or sonar pings and in one cases to create an ultrasonic micro-heater for cauterization [72]. Other applications include energy converters in the form of harvesters [27], and others make use of ferroelectricity by means of polarization reorientation to create non-volatile computer memory [7]. However the focus of the testing equipment which will be discussed in this thesis is for structural applications. While the coupling of ferroelectric materials allow for uses in actuators and sensors, it also allows for the dissipation of energy, via another outlet (i.e. mechanical energy can be dissipated as electrical or thermal energy), allowing for the creation of devices that can either passively or actively damp vibrations. Such devices have a wide range of potential applications, specifically in aerospace applications where the ability to damp out vibrations in plane, jet, and satellite structures is desired.

1.4. PREVIOUS EXPERIMENTATION ON FERROELECTRIC MATERIALS

In the following, existing experimental techniques for characterizing ferroelectrics will be reviewed, in particular, the first section will discuss experiments with a focus on measuring electrical properties, the second will focus on mechanical property testing and the third will focus on measuring the influence of temperature. There is inherently overlap in testing between the three sections however this will reveal the gap in empirical data that our new apparatus can be used to fill.

1.4.1. Experiments Measuring Electrical Properties. Currently an important area of applications for piezoelectrics and specifically ferroelectrics is in electronics, and this has resulted in a large quantity of experimental data on the electronic properties of ferroelectrics. These experiments include testing the polarization switching time for possible uses as a fast relay switch [41], and measuring the polarization fatigue to increase the life expectancy of memory applications[65, 18]. Other properties of interest include electrical creep [78], ultra high frequency dielectric properties [63], the ability to enhance the electrical properties through manufacturing or post processing [6, 13, 56], and depolarization-field-induced instability [77].

1.4.2. Experiments Measuring Mechanical Properties. A large amount of experimental data on the mechanical properties are also available due to the widespread application of ferroelectrics in sensors and actuators. To understand the mechanical properties, researchers have developed experiments from the nanoscale to the macroscale, testing shockwave compression [60] and the electric energy generated by shock compression [46], fatigue [85] and fracture [83] of ferroelectric ceramics, high temperature mechanical properties [17], bulk material characterization [50], and nanoscale studies of individual ferroelectric domains [26]. While there are many mechanically based experiments, the ones which are most relevant to this study are those which measured mechanical damping in ferroelectrics.

As stated before, piezoelectric and ferroelectric materials are used for both active and passive vibration damping in structures. Passive damping methods used in dissipating mechanical energy make use of the thermomechanical coupling and/or the electromechanical coupling. This is done by converting the mechanical energy into another form of energy which can be more easily dissipated from the system. For the passive damping that utilizes thermomechanical coupling, ferroelectric inclusions can be used in a matrix with a high coefficient of thermal conductivity. This allows the thermal energy produced by the domain wall motion of the ferroelectric to be dissipated throughout the material

[36]. Other passive methods use the electromechanical coupling to dissipate mechanical energy through an electrical circuit. This can be done using a resistor in series with the ferroelectric or by using a conductive matrix composite in which the matrix itself acts as the shunt resistor in series with the ferroelectric to dissipate the energy via joule heating [2, 3, 35]. Semi-passive methods have been developed such as synchronized switch damping in which a similar circuit to the shunt resistor is used but this method incorporates a half period pulse switch and an inductor. The switch, attached to a sensor, is closed when the displacment extremes are detected, and the RLC circuit is discharged and dissipates energy via heat as shown in Figure 1.9 [42]. Actively controlled methods include those that work by applying an external voltage to cancel out vibrations, or controlling the temperature and the phase of the material is used to control damping [54]. These methods have tradeoffs, the passive methods are low in complexity compared to actively damped methods, however actively damped methods achieve a loss tangent approximately an order of magnitude larger [22, 4, 12]. Actively controlled methods are inherently more complex and are limited by the force and strain constraints of piezoelectricity.

1.4.3. Experiments Measuring the Influence of Temperature. Experiments focusing on the thermal properties of pyroelectrics have been performed, measuring the pyroelectric effect along with thermal expansion and thermal strain [61, 67, 37]. Pyroelectrics are commonly used to accurately measure temperatures from a distance. With this currently being an important application, thermography experimentation is extensive [69, 31, 45, 23, 29]. Previous experiments of interest in this study are ones that have been performed at low or cryogenic temperatures. These studies tend to be with smaller samples, typically thin film or single crystal specimens. The reason for this is practicality; it is faster and less costly to cool down a smaller setup than it is to cool down a larger setup. These studies have led to discoveries of ferroelectric properties in materials such as $SrTiO_3$ and $KTaO_3$ which have a Curie temperature below that of room temperature, e.g. $SrTiO_3$, which has a Curie temperature of 3.0 K [33]. Experiments characterizing the dielectric and

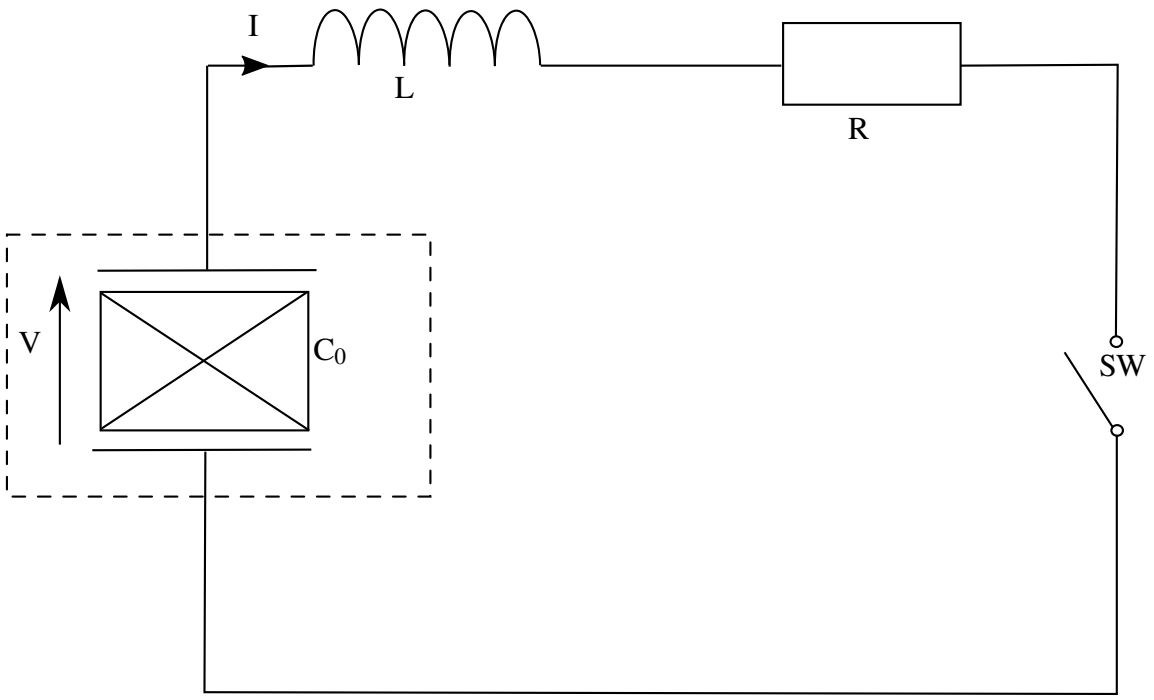

Figure 1.9. Circuit model for synchronized switch damping [42].

piezoelectric properties of ferroelectrics at cryogenic temperatures have been performed for a variety of materials including, PZT, barium titanate ($BaTiO_3$), lanthanum-doped lead zirconium titanate (PLZT), barium strontium titanate (BST), and lead zinc niobate-lead titanate (PZN-PT) [51]. Academic research on testing materials at cryogenic temperatures is not new, however researchers and engineers are currently tasked with designing equipment and structures for cryogenic environments, such as deep space, which require structures to operate at temperatures as low as 2.726 K [21]. Current experiments at cryogenic temperatures have involved testing materials for applications in stack actuators, or displacement testers [28, 66, 80], thermometry sensors, as well as other sensor experiments [20, 53]. Testing materials in their application environment enables engineers to properly test their designs before putting them into the field, or in this instance into space.

1.5. MOTIVATION

While ceramics typically have a relatively high Young's modulus and low damping coefficient, polymers have a relatively large damping coefficient but a low Young's modulus, and metals typically have a moderate Young's modulus and damping coefficient, the ideal material for some structural applications would have both high damping and high Young's modulus. As previously stated ferroelectric ceramics have been used as energy absorbers that are controlled both passively and actively, and have stimulated this study. Other studies, which directly motivated the design of this new experimental equipment, have looked into viscoelasticity of ferroelectrics both under small and large electric fields and have shown that ferroelectric ceramics can be electrically stimulated in order to increase the mechanical damping [73, 74]. These applications allow for a ceramic (with high Young's modulus), to have a damping coefficient comparable to that of some polymers [4, 9]. Correlating to the recent studies, new equipment has been designed in pursuit of being able to test the viscoelastic properties of ferroelectric ceramics under large electric fields [38], however there are still limitations to these testing apparatuses, as will be discussed in the next section. The design goal of this experimental apparatus was to control mechanical, electrical, and thermal fields in order to be able to fill in the gaps that still exist in the experimental data.

1.6. OUTLINE OF THESIS

Now that the introduction to ferroelectrics, background, and motivation have been established, the outline of this thesis is given in the following. In the next chapter, the reasoning and development of the equipment will be examined, then the results from the preliminary experiments will analyzed and discussed. Lastly, the conclusion will summarize what this project accomplished and suggestions for future work and improvements will be given.

2. REQUIREMENTS AND DESIGN OF EQUIPMENT

An experimental setup for measuring the electromechanical response in a simulated space environment requires a vacuum system, the ability to cool the setup down to cryogenic temperatures, as well as the ability to simultaneously apply both electrical and mechanical loading. For characterizing the time-dependent properties (e.g. viscoelastic properties and fatigue), electric fields and mechanical loads must also be applied dynamically over wide ranges of frequency. Each section of this chapter will cover a design requirement and the development and implementation of a solution, culminating in the creation of the cryogenic broadband electromechanical spectroscopy (CBES). This CBES will then be compared to preexisting experimental setups and improvements and modifications will be addressed.

2.1. MECHANICAL LOADING

There are existing methods for applying dynamic mechanical loading to materials, which have been reviewed in e.g. [74]. These viscoelastic measurement techniques include dynamic mechanical analysis (DMA), inverted torsion pendulum (ITP), acoustic resonance spectroscopy (ARS), and broadband viscoelastic spectroscopy (BVS). However, these methods have drawbacks or inherent traits that eliminate them as viable options for testing ferroelectric ceramics. DMA for example usually operates below 1000 Hz, and is limited to materials with a modulus of elasticity of less than 1 GPa [47]. Also, they require a fixed-fixed configuration, which is suitable for some materials (i.e. polymers), this adds difficulties with ferroelectrics and ceramics due to piezoelectric strain and brittleness, respectively. The ARS can apply a wide range of frequencies, from 20 Hz to 30 kHz, however ARS uses piezoelectric transducers to stimulate and sense the vibrations ([62]). The use of these piezoelectric transducers and sensors would interfere with the application of an external electric field to the specimen, or conversely the application of an external electric

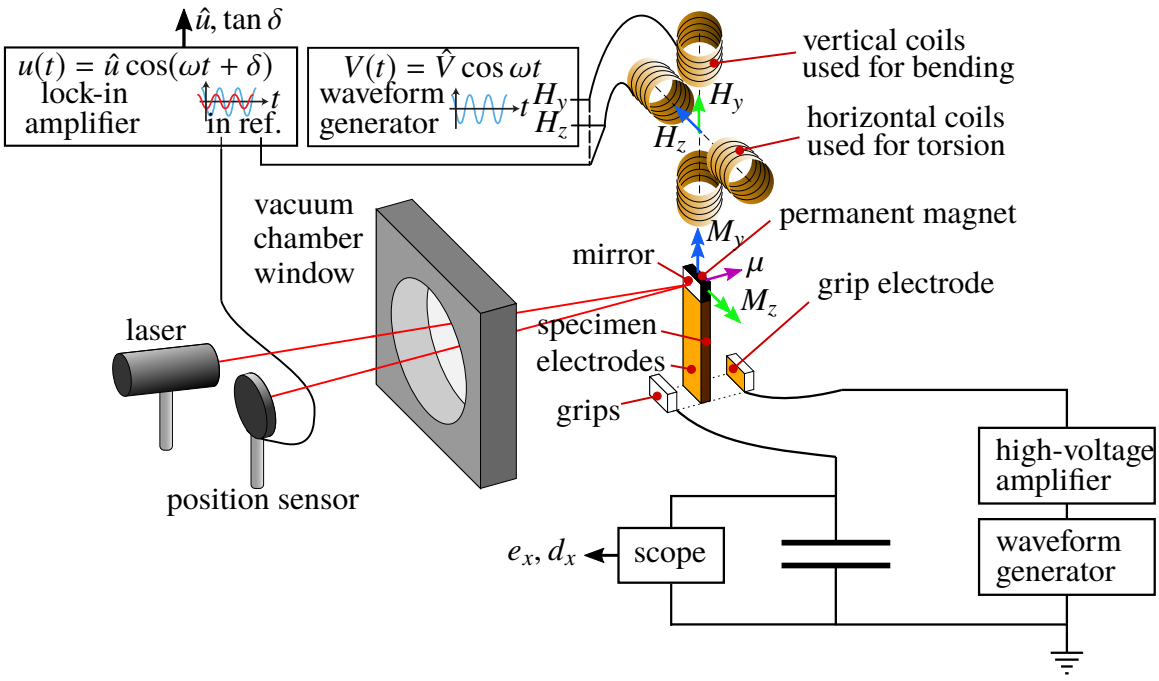

Figure 2.1. Schematic of the BES setup [75].

field to the specimen would interfere with the actuation and sensing capabilities of the ARS. The ITP method encapsulates the basic idea that is desired, using fixed-free, contactless, loading and measurement. However the frequency range for The ITP setup is 10^{-5} to 10 Hz [34, 49], which may be too slow to study the effects of polarization switching on mechanical damping. The BVS, also a fixed-free test setup, the ability to be placed under vacuum, and allows for both torsional and bending measurements to be tested within a frequency range of 10^{-6} to 10^{5} Hz as reported by [40]. The BVS allows for a wide range of forcing frequencies to be applied while allowing for the possibility of other methods to apply electrical loading as done so by [75] in the creation of broadband electro-mechanical Spectroscopy (BES). The need for contactless actuation and measurement stems from the material being tested. As the material is a ceramic it is inherently brittle, and therefore makes a double cantilever or fixed-fixed testing setup impractical. Also the fixed-free setup allows for expansion from both thermal and electrical loads which will be present in this type of testing.

The BES, as shown in Figure 2.1, is the most relevant, state of the art, equipment for this study. The BES setup allows for a fixed-free testing setup with contactless actuation and measurement while maintaining the ability to apply electric fields to the specimen. In the BES the waveform generator outputs a sinusoidal voltage of amplitude $\hat{V}$ and a frequency of ω to the Helmholtz coils. The coils produce a magnetic field for the bending H_y or torsion H_z, which interact the the permanent magnet dipole μ to apply a moment M_y or M_z, respectively. The waveform generator amplified by a high-voltage amplifier is used to apply electric fields e_x to the specimen in series with a Sawyer-Tower circuit to measure the electric displacement d_x. The lock-in amplifier takes a reference signal from the waveform generator and an input from the laser position sensor and uses phase sensitive detection to measure the amplitude $\hat{u}$ and phase shift δ. The moment is induced through the magnetic field H generated by the Helmholtz coils, which is given by

$$H = \frac{\mu_0 n I}{\sqrt{8} R}, \tag{2.1}$$

and its interaction with the dipole m of the permanent magnet through

$$\tau = \mu_0 m \times H, \tag{2.2}$$

where μ_0 is the relative permeability of a vacuum ($4\pi \times 10^{-7}$ H/m), n is the number of turns of the coil, I is the current through the coil, R is the radius of the coils and the coil distance from the magnet, and m is the magnetic moment([16]).

The current is supplied by a waveform generator producing a sinusoidal voltage output. The limited power output of the waveform generator, which is typically in the 10-100 mW range, limits the magnitude of the applied moment. To circumvent this limitation, an amplifier circuit was added such that the waveform generator provides the input signal and the amplifier circuit isolates the current draw to an external power supply, allowing for a greater current to be input to the coils. Both BES and BVS, use a similar laser, mirror,

and laser position sensor to detect the deflection of the specimen tip. This has been proven to be an effective method for contactless tip deflection measurement and can be performed inside of a vacuum chamber [38, 19]. To determine the loss tangent and dynamic Young's modulus, a lock-in amplifier was used. Utilizing dual phase-sensitive detection (PSD), the lock-in takes a reference signal (from the waveform generator),

$$V_{ref} \sin(\omega t + \theta_{ref}), \tag{2.3}$$

and an input signal (from the laser position sensor),

$$V_{in} sin(\omega t + \theta_{in}), \tag{2.4}$$

to measure the in-phase component,

$$X = V_{in} \cos\theta, \tag{2.5}$$

where

$$\theta = (\theta_{in} - \theta_{ref}), \tag{2.6}$$

ω is the frequency, V_{ref} is the amplitude of the reference signal, and V_{in} is the amplitude of the input signal, and θ_{ref} and θ_{in} are the reference and input signal phases, respectively. The second PSD component shifts the reference signal by 90°, i.e.

$$V_{ref} \sin(\omega t + \theta_{ref} + 90^{\circ}), \tag{2.7}$$

to measure the quadrature component,

$$Y = V_{in} \sin\theta, \tag{2.8}$$

which allows for the amplitude,

$$R = \sqrt{(X^2 + Y^2)} = V_{in}, \tag{2.9}$$

and phase shift (angle),

$$\theta = \tan^{-1}\left(\frac{Y}{X}\right), \tag{2.10}$$

to be calculated. This method has been used to determine the loss tangent and dynamic Young's modulus of the materials in BES by measuring the phase shift between stress and strain and amplitude, respectively. Since the reference signal is the voltage signal from the waveform generator, and the coils are inductors there is an inherent phase shift between the voltage and current in the coils. For the BES setup this was corrected for using a magnetometer and calibrating the frequency response of the Helmholtz coils. In an attempt to avoid the need for a calibration, the current through the coils was measured directly (by the voltage drop across a 1 Ohm resistor), and used as the reference signal for the lock in amplifier similarly to the BVS [19]. However this led to discrepancies in the phase shift measurements, varying based on the voltage applied to the Helmholtz coils. Thus, similarly to the BES, a calibration using a magnetometer was performed for room temperature tests (see Figure 2.2). Following Faraday's law, the induced emf, measured as a voltage $V_{out}(t)$, is a function of the rate of change in the magnetic flux $\frac{\Delta B}{\Delta t}$ produced by the Helmholtz coils, given by

$$emf = V_{out}(t) = nA\frac{\Delta B(t)}{\Delta t}, \tag{2.11}$$

where n and A are the number of turns and area of the magnetometer. Since the magnetic field is a sinusoidal function of the current I, the derivative shifts the the phase 90°, such that

$$B(\omega t + \delta_{coils}) \propto I(\omega t + \delta_{coils}), \tag{2.12}$$

and

$$emf = V_{out}(\omega t + \delta_{coils}) \propto B(\omega t + \delta_{coils} + 90°) \propto I(\omega t + \delta_{coils} + 90°), \tag{2.13}$$

allowing for the frequency response of the coils δ_{coils} to be measured. This phase measurements allow for the material loss tangent to be found using (2.6) and setting

$$\theta = \delta_{material} + \delta_{coils}. \tag{2.14}$$

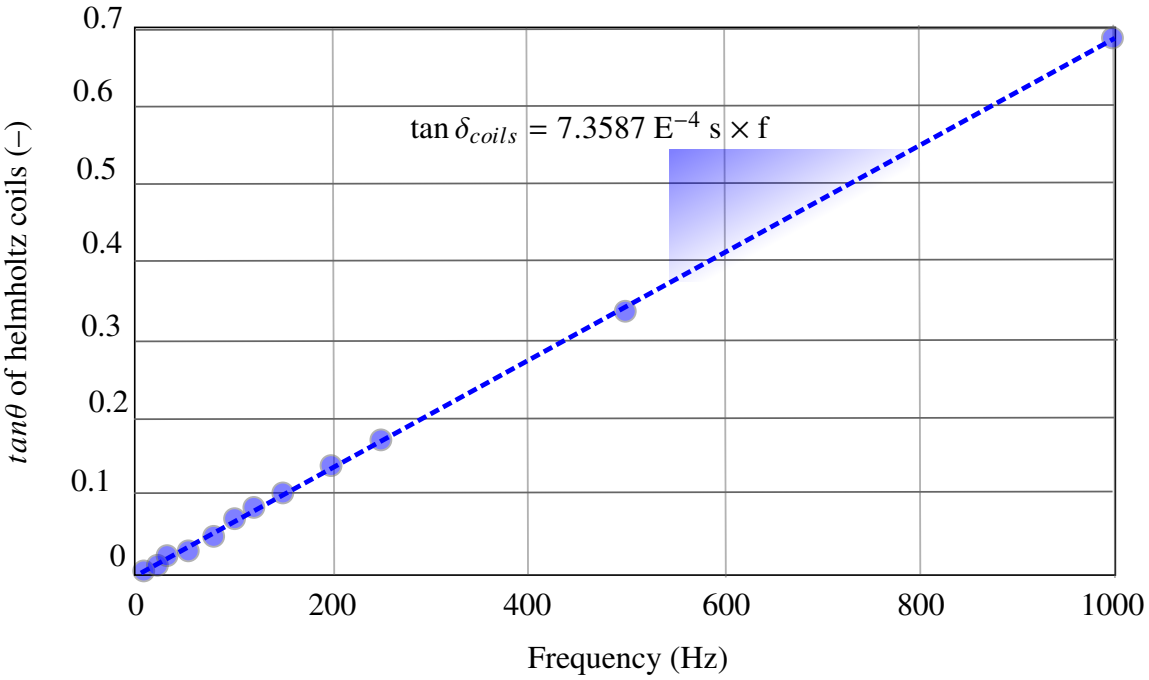

Figure 2.2. tan δ_{coils} of the applied voltage and the produced magnetic field of the vertical Helmholtz coils at room temperature.

However since the temperature is varied in the CBES, a calibration was necessary at every temperature the specimen was tested. To this end, a magnetometer was attached to the coil fixture to allow for the frequency response of the coils to be measured at any temperature. The magnetometer is a 10-turn .25" radius coil in an open circuit. The two leads allow for measurement of the induced emf as an open circuit voltage measurement.

The reduced area and number of turns (as compared to the Helmholtz coils) prevent the magnetometer from interfering with the magnetic field produced from the Helmholtz coils via back emf. The Young's modulus is measured based off of the tip-deflection of the specimen. Similarly to the BVS and BES, the specimen is under an applied stress in the form of an end moment. With a laser incident on the mirror at the end of the specimen, the angle of tip-deflection (θ_{tip}) can be measured by

$$\tan\theta_{tip} = \frac{u_z}{l} \tag{2.15}$$

where u_z is the measured displacement of the laser at the laser position sensor and l is the distance from the laser position sensor to the specimen. Since the specimen is subjected to small deflections, the approximation, $\theta_{tip} \approx \frac{u_z}{l}$, can be used. The deflection of a slender beam under an applied moment, M, is

$$\theta_{tip} = \frac{ML}{EI}, \tag{2.16}$$

where L is the beam length, E is the modulus, and I is the bending moment of inertia. With the moment a function of the current, as shown by (2.2), and the other values known, the dynamic modulus can be expressed as

$$E^* = A\frac{\hat{I}}{\hat{u_z}}, \tag{2.17}$$

where A is a constant composed of the atemporal terms from (2.2) and (2.2), $\hat{I}$ is the amplitude of the current through the coils, and $\hat{u_z}$ is the amplitude of the laser displacement. Figure 2.3 shows the CBES schematic with the waveform generator supplying the reference signal to the lock-in amplifier, and to the current isolation amplifier which drives the coils. The lock-in amplifier uses dual PSD to measure the the amplitude of deflection as well as the phase between the reference signal and the laser position sensor, allowing for the

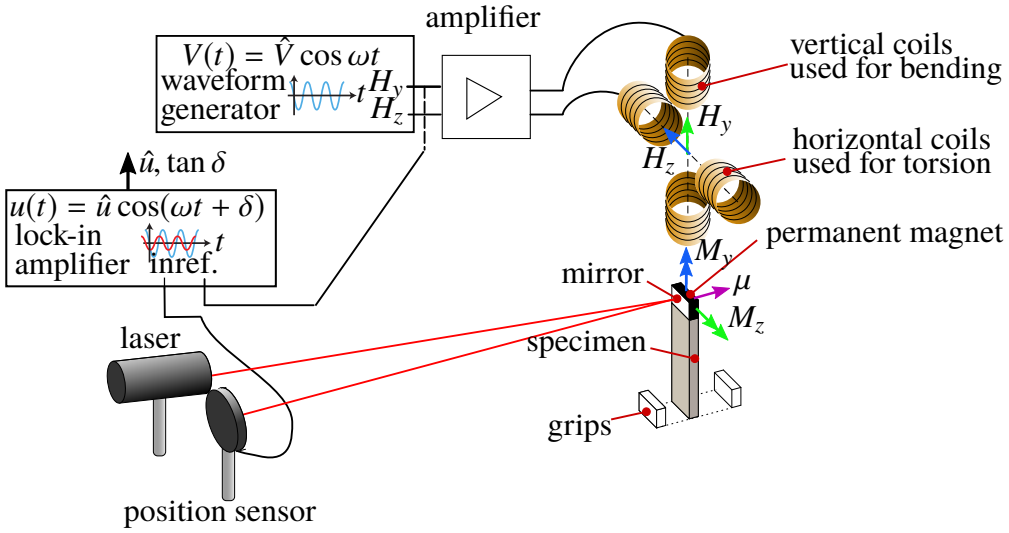

Figure 2.3. CBES Mechanical setup, adapted with permission from Wojnar [74].

dynamic Young's modulus and material loss tangent to be determined. The amplitude and phase are recorded by an oscilloscope concurrently with the electrical loading, as will be discussed in the next section. The specific instruments used are: laser (REO Inc., 633 nm, 5.0 mW) , optical beam position sensor (Newport OBP, 9 mm × 9 mm), lock-in amplifier (SR830 from Stanford Research Systems), waveform generator (TekTronix AFG3022c), oscilloscope (Tektronix MDO 3014), pair of Helmholtz coils (each coil 150 ±1 turns, radius of .5", 32 AWG magnetic wire), current isolation amplifier (See A), and a N38SH Neodymium magnet (.25" × .25" × .1" with a maximum pull of 1.7 lbs at 298 K). For pictures of the actual set-up see Appendix A.

2.2. ELECTRICAL LOADING

While domain wall motions occur under relatively small applied electric fields, the specific case that is desired to be studied is domain switching. Domain switching as previously described, happens in ferroelectric materials under an applied electric field larger than the coercive field. The coercive field of PZT can be as high as 20 kV/cm [30], meaning

it is necessary to apply a high voltage to the specimen safely and without arcing. This requires specially designed grips that can apply an electric potential across test specimens in a safe manner and without electrical arcing. Applying the high voltage is necessary to induce domain switching, but to be able to determine how the domain switching affects damping, the electric displacement of the PZT needs to be measured in-situ. This requires that the electric displacement of the specimen be measured concurrently to the applied electric field and dynamic mechanical properties. The electrical displacement is measured via a Saywer-Tower circuit [58] connected in series to the specimen. This is a commonly used technique which allows the electric displacement (D) of the specimen to be calculated through

$$D = \frac{C \cdot V_{cap}}{SA}, \tag{2.18}$$

where C is the capacitance of the capacitor, V_{cap} is the voltage across the capacitor, and SA is the surface area of the specimen. As shown in Figure 2.4, a high-voltage amplifier in conjunction with the waveform generator are used to supply the high voltage necessary for domain switching. The applied electric field (E_{app}) to the specimen is related to the applied voltage (V_{app}) by the thickness of the specimen (h) by,

$$E_{applied} = \frac{V_{app}}{h}. \tag{2.19}$$

The voltage across the capacitor and the output voltage from the high voltage amplifier are recorded by the same oscilloscope as mentioned in the section above. This allows for the simultaneous measurement of the electric displacement, applied electric field, dynamic Young's modulus, and loss tangent.

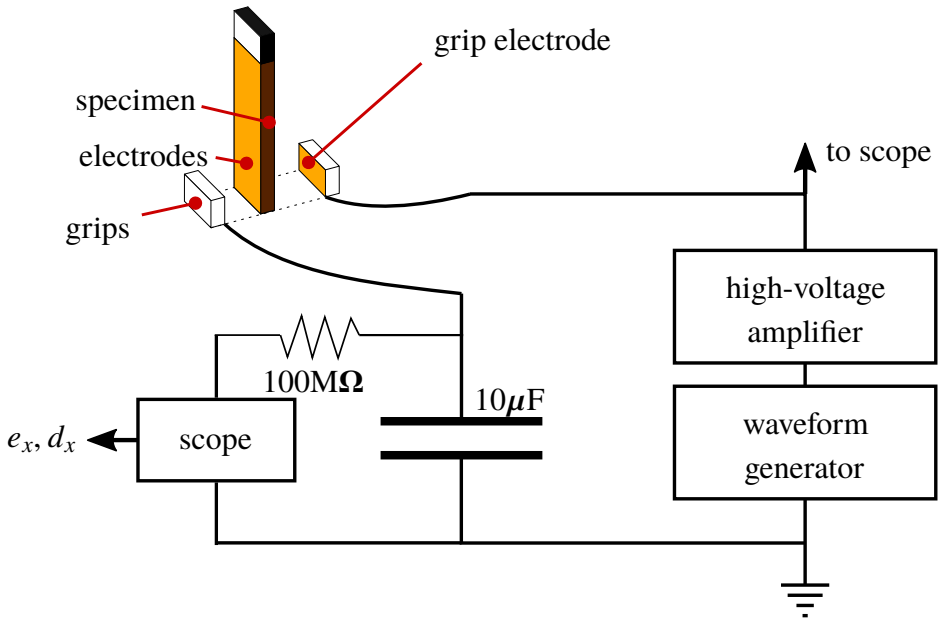

Figure 2.4. CBES Electrical setup, adapted with permission from Wojnar [74].

2.3. THERMAL LOADING

To determine and understand the electromechanical behavior of ferroelectrics in a space environment, specimens must also be tested at cryogenic temperatures. Cryostats, which are devices for reaching and controlling temperature at cryogenic levels, are commercially available and typically work in one of two main ways. Cryogenic temperatures can be achieved by submerging a specimen or apparatus into a cryogen (e.g. liquid oxygen, liquid helium, or liquid hydrogen) or pouring the cryogen over the test apparatus. These styles of cryostats are commonly referred to as wet cryostats due to the the specimen or apparatus coming into contact with the cryogen. Wet cryostats are used for various reasons, either making use of the superconductivity of the cryogen, or the ease of use of the device in being able to submerge the whole setup into the cryogen. However to perform a mechanical test the cryogen itself could pose a problem of increased noise and measurement difficulties. The other common type of cryostat is called a dry cryostat, this method still uses cryogen, however the cryogen never comes into direct contact with the test setup. Instead the way dry

cryostats work is by pumping the cryogen onto a platform for the test apparatus consisting of a material with high thermal conductivity commonly referred to as the cold head. This allows the cold head to act as a heat sink to the test apparatus and conduct heat away from the sample to the cold head. The cryogen then carries the thermal energy away in the evaporation process. The complete process uses a pump to maintain the flow of cryogen over the cold head. The pump may add noise, so the design must incorporate a cryostat that can reach a cryogenic temperature and temporarily be turned off (while maintaining the desired temperature) during the electromechanical testing.

To test ferroelectrics at cryogenic temperatures, a custom designed cryostat from Janis Research Company was built. This system is a closed-cycle helium system, which means that the cryogen (liquid helium) will never come into contact with the test apparatus, but will flow to a cold head which acts as the base for the test apparatus. The cryostat chamber has optical ports allowing for the laser position measurement system. A custom cartridge heater, and calibrated GaAlAs temperature sensor diode, located at the base of the cold head and on the specimen grip, respectively, are used with a LakeShore Model 335 temperature controller to set the temperature of the test apparatus platform within ±0.005 Kelvin. The test platform itself is made from brass and is at the maximum thickness the manufacture could make, .5" thick, to insure the maintenance of the temperature after the cryogen pump (Sumitomo HC-4E1) was shut off. Also to accommodate the mechanical loading and measure the deflection, optical ports were installed into the chamber of the cryostat. To be able to test different length specimens, two 2" diameter optical ports were put in the chamber 180° apart and vertically offset 1.5" such that the cryostat could be rotated allowing for the appropriate port to test specimens from .5" to 3.5" in length.

2.4. VACUUM REQUIREMENTS

Space is a vacuum, and to simulate that in a lab inside the Earth's atmosphere, a vacuum chamber and an accompanying pump are required. Space applications range in pressure from about 10^{-4} Torr to 10^{-11} Torr on the moon and tends towards 0 Torr in deep space [55]. Besides simulating the space environment, the vacuum chamber provides several additional benefits to the experimental setup. For mechanical loading, placing the sample under vacuum will reduce any parasitic damping due to the air resistance. The parasitic damping due to surrounding air on a cantilever is proportional to the pressure and to the density of the air as shown by Chen et al. [10] through the equation,

$$\tan \delta_{air} = \frac{2P}{\pi \rho c} \sqrt{\frac{C_p \mu}{C_v R T}} \tag{2.20}$$

Where C_p and C_v are heat capacity under constant pressure and volume respectively, ρ is the density of the solid, μ is the density of the fluid (air), c is the speed of sound in the solid and P, R, and T correlate to the pressure, gas constant and temperature, respectively. As shown by (2.20), the lower the pressure and density, the lower the parasitic damping due to the fluid.

Another aspect of the vacuum system is that it affects electrical arcing; the breakdown voltage required for arcing a gap in air varies with pressure. To understand the correlation between a vacuum and arcing one can look at Paschen's law, [43] and the voltage breakdown, V_b, equation

$$V_b = \frac{Apd}{\ln pd} + B, \tag{2.21}$$

where A and B are constants that depend on the medium in the spark gap, p and d are the pressure of the surroundings and the distance between the two electrodes, respectively [52]. Figure 2.5 shows that the breakdown voltage is not linear with respect to pressure and the

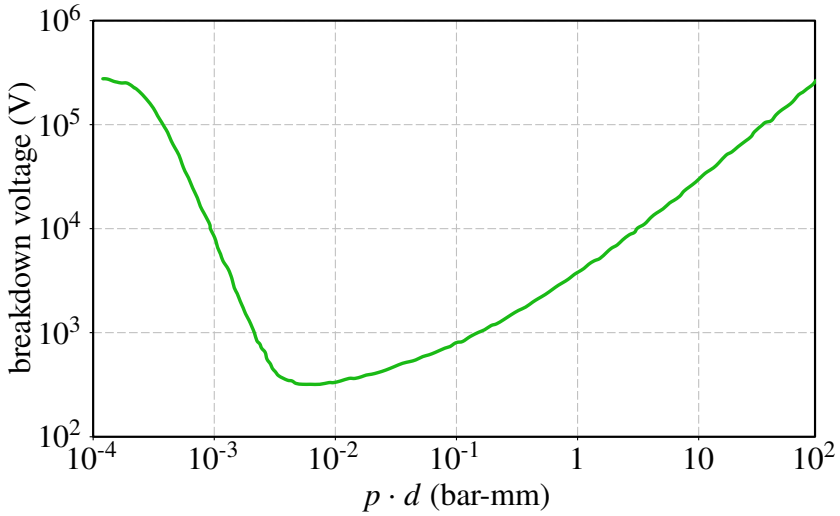

Figure 2.5. Voltage breakdown versus pressure-distance (Paschens curve) in air [52].

ideal pressure with respect to electrical loading would be less than 10^{-3} bar-mm or greater than 10 bar-mm. Due to the geometry of the specimens, and the voltage applied in this study our experimental set-up this requires a pressure of 10^{-4} bar or greater than 1 bar-mm.

Most cryostats need to be placed under vacuum in order to function properly. The custom cryostat by Janis required an evacuated pressure of 10^{-4} mbar or less. The lower the pressure the quicker the cooldown time. For this experimental set-up the maximum allowable pressure is determined by the cryostat 10^{-4} mbar, but with respect to every type of loading (mechanical, electrical, and thermal), a pressure lower would yield more efficient and accurate experimental equipment. To achieve the desired pressure an Edwards T-Station 75 vacuum pump is used. This vacuum system has an ultimate pressure of $< 4 \times 10^{-7}$ mbar. For experiments, typically pressures below 1.1×10^{-7} bar are reached, which is sufficient for all loading conditions.

Table 2.1. Comparison of BVS, BES, and CBES viscoelastic characterization methods.

method	**bandwidth**	**moduli**	**temp.**	**e-field**	**vac.**	**contactless**
BVS	10^{-6} to 10^{5}	up to 10^{4} GPa	up to 160°C	–	–	✓
BES	10 to 10^{4} Hz	up to 10^{4} GPa	up to 400°C	✓	✓	✓
CBES	10 to 10^{4} Hz	$> 10^{4}$ GPa	-243 to 50°C	✓	✓	✓

2.5. CRYOGENIC BROADBAND ELECTROMECHANICAL SPECTROSCOPY

All of these subsystems together create the Cryogenic Broadband Electromechanical Spectroscopy setup (as shown in Figure 2.6). Functionally any load can be applied individually, and all loads can be applied simultaneously, which is the true benefit of this testing apparatus. The CBES allows for the measure of dynamic mechanical, and electrical properties, with the added ability of being able to measure the influence of cryogenic temperatures on these dynamic properties (see Table 2.1). While all methods allow for a wide range of viscoelastic materials to be tested in a contactless manor, however the CBES is the only method which allows this to be done at cryogenic temperature while being able to apply simultaneous high voltage electrical loading. For images of the actual CBES set-up and ancillary equipment please see Appendix A.

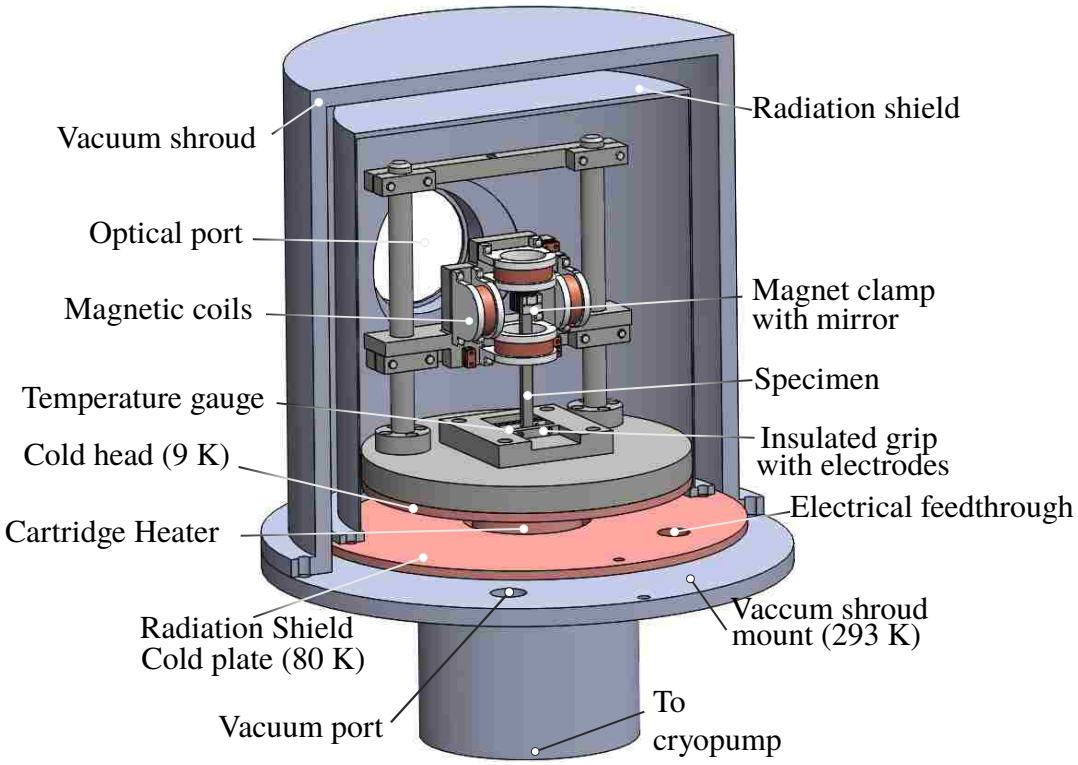

Figure 2.6. Cryogenic broadband electromechanical spectroscopy.

3. VALIDATION AND EXPERIMENTATION

The experimental setup developed enable the measurement of the dynamic modulus, loss tangent, and electric displacement hysteresis under large electric fields at cryogenic temperature, which was not possible with previous equipment. As a first step, the experimental setup will be used to measure known properties of well characterized materials. Specifically the mechanical properties of aluminum 6061-T6 and the electrical properties of PZT. Then electromechanical tests at room temperature will be performed on PZT. This room temperature tests are compared to literature in order validate the accuracy of the setup. Then, experiments carried out at cryogenic temperatures are reported and obsevrations are made with regards to the effects of low temperature on material properties. An important note is that the Young's modulus will be reported as relative Young's modulus such that comparisons can be made to literature [75, 39, 74]. This relative Young's modulus is the measure of the instantaneous amplitude of deflection with no applied electric field u_z^0 over the amplitude of the deflection when a field is applied u_z, as shown by

$$\frac{E}{E^0} = \frac{u_z^0}{u_z}, \tag{3.1}$$

where the E is the dynamic Young's modulus and E^0 is the dynamic Young's modulus with no applied electric field.

Table 3.1. Properties of PZT-5A4E obtained from Piezo Systems Inc.

parameter	**symbol**	**value**	**units**
density	ρ	7.8	g/m^3
coercive field	E_c	1.2×10^6	V/m
axial elastic modulus	Y_3	5.2×10^{10}	N/m^2
transverse elastic modulus	Y_1	6.6×10^{10}	N/m^2
piezoelectric coefficients	d_{33}	390×10^{-12}	m/V
	d_{31}	-190×10^{-12}	m/V
Curie temperature	T_c	350	$^\circ C$
thermal expansion coefficient		4×10^{-6}	$^\circ$C^{-1}
mechanical quality	Q	80	–
composition		60 – 70	% lead oxide
		5 – −25	% zirconium oxide
		5 – −15	% titanium oxide
		0 – −4	% lanthanum oxide
		0 – −20	% zirconium oxide
		0 – −7	% nickel oxide

3.1. MATERIAL PROPERTIES

The PZT specimens used in the experiments were model PSI-5A4E from Piezo Systems Inc., an industry type 5A piezoceramic, pre-plated with nickel electrodes, and pre-poled through the thickness direction. The specimen dimensions are 1.016 mm (0.04") thick, 3.175 mm (0.125") wide, and 38.1 mm (1.5") long. The properties provided by the manufacture are shown in Table 3.1.

Poled PZT is transversely isotropic, as can seen by the different axial and transverse elastic moduli in the Table 3.1. To this end, the Young's modulus referred to in this report will be that of the transverse modulus, denoted as Y_1 by Piezo Systems Inc.

Table 3.2. Properties of the aluminum cantilever beam

parameter	**symbol**	**value**	**units**
density	ρ	2.7	g/cm^3
complex Young's modulus	E^*	$69(1 + .005i)$	GPa
cross-sectional area	A	0.05162	cm^2
area moment of inertia	I	3.335×10^{-5}	cm^4
end mass	m	1.89	g
beam length	L	6.05	cm

3.2. VALIDATION

In order to asses the accuracy of the experimental setup, a series of experiments were carried out at room temperature (with both PZT and aluminum), where the resulting data can be compared with existing data and models. To this end, the dynamic Young modulus and loss tangent of aluminum, which is well characterized, was measured. Then, the electric displacement hysteresis of PZT was measured and compared to literature. Finally, the dynamic modulus and loss tangent of PZT under cyclic electric fields at room temperature was measured and compared with previous experiments.

3.2.1. Determining the Accuracy of the Modulus and Loss Tangent Measurements. To verify that the Helmholtz coils and the laser-detector setup used for measuring dynamic Young's modulus and loss tangent was accurate, a well characterized material was tested, viz. aluminum 6061-T6. Specimens were .89 mm (0.035") thick, 5.715 mm (0.225") wide, and 64.29 mm (2.531") long. The specimen's dynamic Young modulus and loss tangent was measured using CBES for frequencies from 2 Hz to 2.5 kHz and compared to theoretical result of a dynamic Euler-Bernoulli beam. The given properties and parameters used in the model are values for 6061-T6 obtained [76] or were directly measured and are shown in Table 3.2.

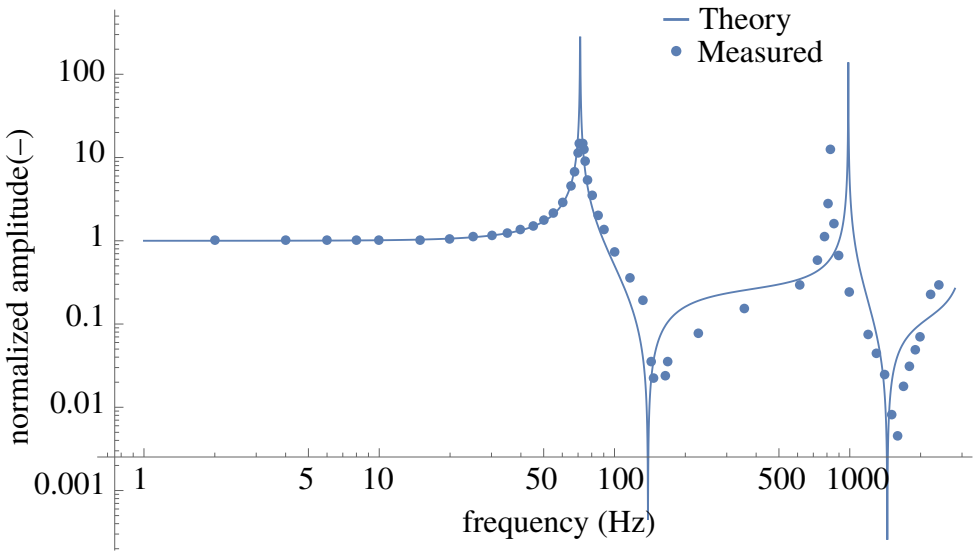

Figure 3.1. Frequency response of 6061-T6 aluminum beam in comparison with dynamic Euler-Bernoulli beam theory.

The boundary conditions for the model were that of a fixed-free beam, with an end mass, subjected to an applied sinusoidal bending moment on the free end. From Figure 3.1, a peak in the relative amplitude is observable at 74 Hz, corresponding to the fundamental frequency, and a relative minimum at 163 Hz corresponding to the first anti-resonance. Each of the following positive and negative peaks correspond to the subsequent resonance and anti-resonance frequencies, respectively. Using the material properties obtained from literature, and measurements taken directly from the aluminum specimen, the model accurately captures the fundamental and first anti-resonance frequency of the aluminum cantilever. Thus, the setup is accurately measuring the dynamic Young's modulus. The higher order resonances are difficult to capture due the the approximations in the model (i.e. point end mass, clamping conditions, and effective beam length).

Besides measuring the dynamic Young modulus, the loss tangent of aluminum 6061-T6 was also measured and compared to literature in order to characterize any parasitic damping and noise in the setup. To capture the material loss tangent, and avoid geometric

dependence, the applied loading was at a sub-resonant frequency of 5 Hz. The applied voltage was used as the reference signal and the corresponding deflection measured by the laser position sensor was used as the input signal, the reference and input signal representing the applied stress and resulting strain, respectively. The phase shift due to the Helmholtz coils, δ_{coils}, (which was measured and shown in Figure 2.2) was subtracted from the total measured phase to obtain the material loss tangent, $\tan\delta_{al}$. The loss tangent measured for aluminum was = 0.005 at 5 Hz, which coincides with values measured from previous experiments, ranging from 0.005 to .019 [76, 81]. The ability to measure the relatively small loss tangent of aluminum provides confidence in the measurement of the loss tangent of PZT which is an order of magnitude larger than aluminum 6061-T6 (see mechanical quality in Table 3.1).

3.2.2. Measuring Electric Displacement Hysteresis. To verify the accuracy of the Sawyer-Tower circuit, a cyclic electric field was applied to PZT specimens and the resulting electric displacement was measured and is shown in Figure 3.2. The measured hysteresis curves were compared with those from the literature.

The electric displacement vs. electric field (P-E) curve in Figure 3.2 demonstrates the hysteresis associated with a ferroelectrics. As the applied field surpassed the coercive field (13 kV/cm), the electric displacement switches and when the applied electric field is removed, the electric displacement will return to the spontaneous polarization value (0.34 C/m^2). The coercive field is in agreement with the approximate value of 12 kV/cm provided by the supplier and the P-E curve resembles those found in literature [70, 84]. This demonstrates the ability of the CBES system to apply coercive electric fields and accurately measure the electric displacement via the Saywer-Tower circuit.

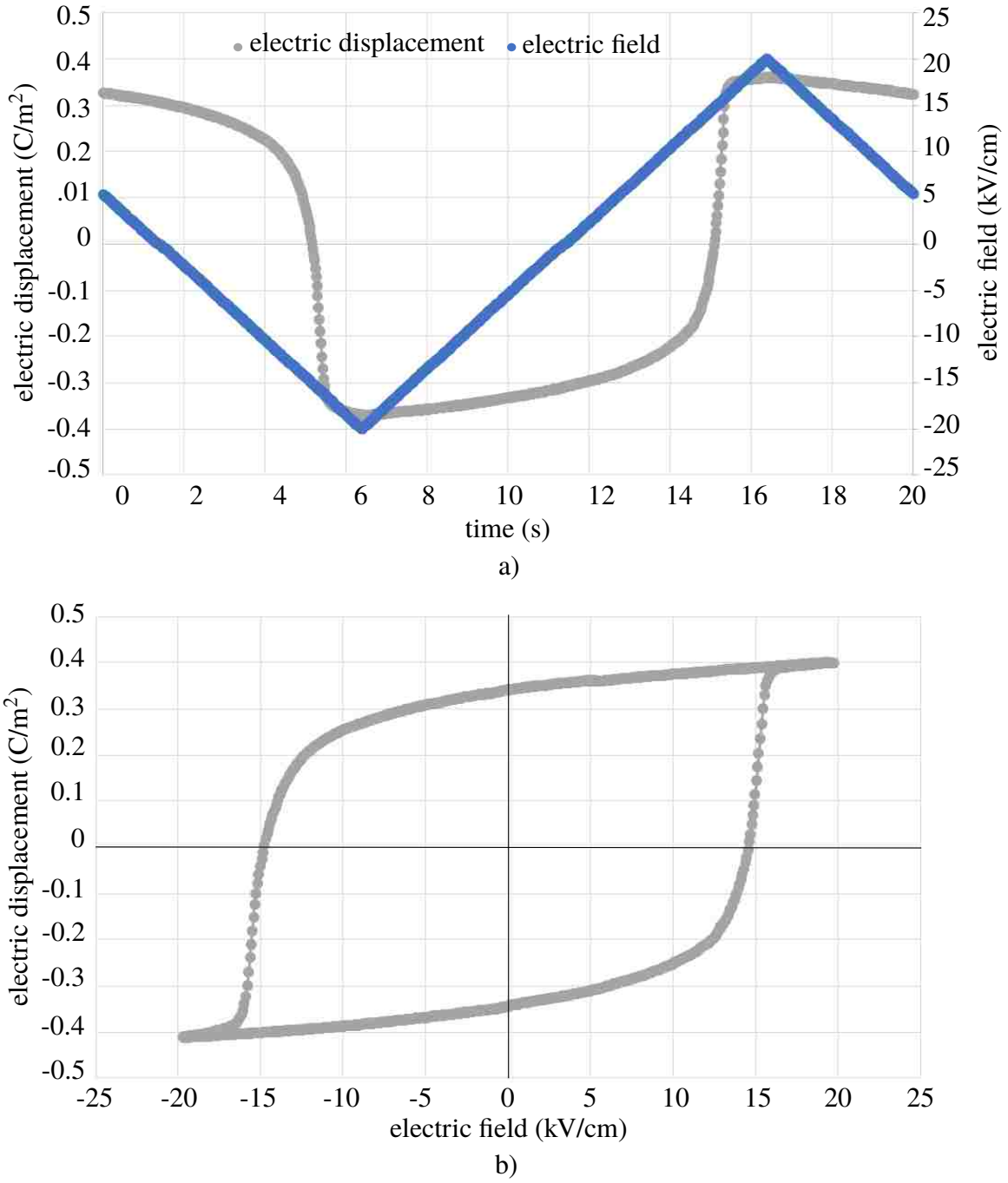

Figure 3.2. a) Concurrent measurements of electric displacement and electric field and b) electric displacement plotted with respect to the electric field; with measurements performed at room temperature and the frequency of the applied electric field was 50 mHz.

3.2.3. Dynamic Modulus and Loss Tangent of PZT at Room Temperature.

The final validation step before testing materials at cryogenic temperatures was to measure the dynamic modulus and loss tangent at room temperature and compare the result with previous experiments. The test follows the methods used by Wojnar [74], the only existing experimental data currently in literature. The test is performed by applying harmonic mechanical loading in the form of a bending moment on the free end of the specimen, while a substantially lower frequency triangle wave electrical field was applied. The loading frequencies of the mechanical and electrical loads are orders of magnitude in difference such that the electric load can be assumed to be quasi-static. This allows for the measurement of dynamic properties during domain switching (and thus domain wall motion). For each test, the mechanical loading was driven by a 5 Vpp (peak-to-peak voltage) sine wave applied to the Helmholtz coils, while the electric field was applied by supplying a 1 Vpp triangle wave at 50 mHz to the high voltage amplifier with a gain of 2000. Four measurements were recorded concurrently (see Figure 3.3): beam deflection amplitude, phase between applied voltage and resulting deflection (allowing for the calculation of the loss tangent), applied electric field, and the charge on the specimen .

The simultaneous measurements allow for the relative bending moment and loss tangent to be observed as the PZT is undergoing domain switching at an applied electric field of 15 kV/cm, as shown in Figure 3.4. The loss tangent was 0.09 at no applied electric field, and reached a maximum of 0.35 at an applied electric field of 15 kV/cm. The relative Young's modulus decreased, as expected, as the loss tangent increases. The dynamic mechanical properties show a drastic difference when a coercive field is applied, with greater than a 375% increase in loss tangent and a reduction of dynamic Young's modulus by 40%. After the domain switching occurs, the loss tangent reaches a minimum value of .045, while the dynamic Young's modulus increases to it maximum of 24% greater than the modulus at no applied electric field. These results are consistent with previous experimental results obtained by le Graverend et al. [39], Wojnar et al. [75].

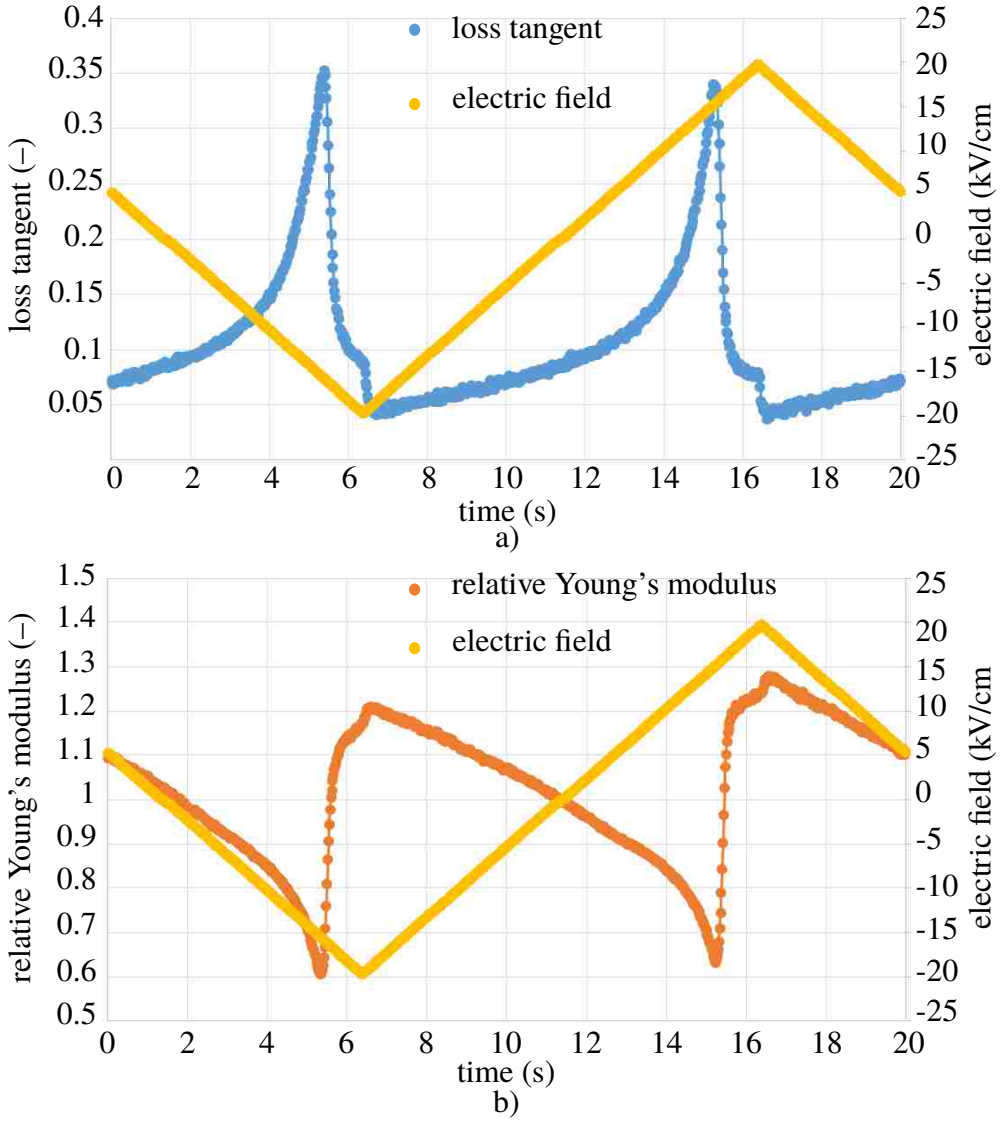

Figure 3.3. Concurrent measurements of a) loss tangent (tanδ) and applied electric field, and b) relative Young's modulus and applied electric field for a single test at a mechanical frequency of 75 Hz.

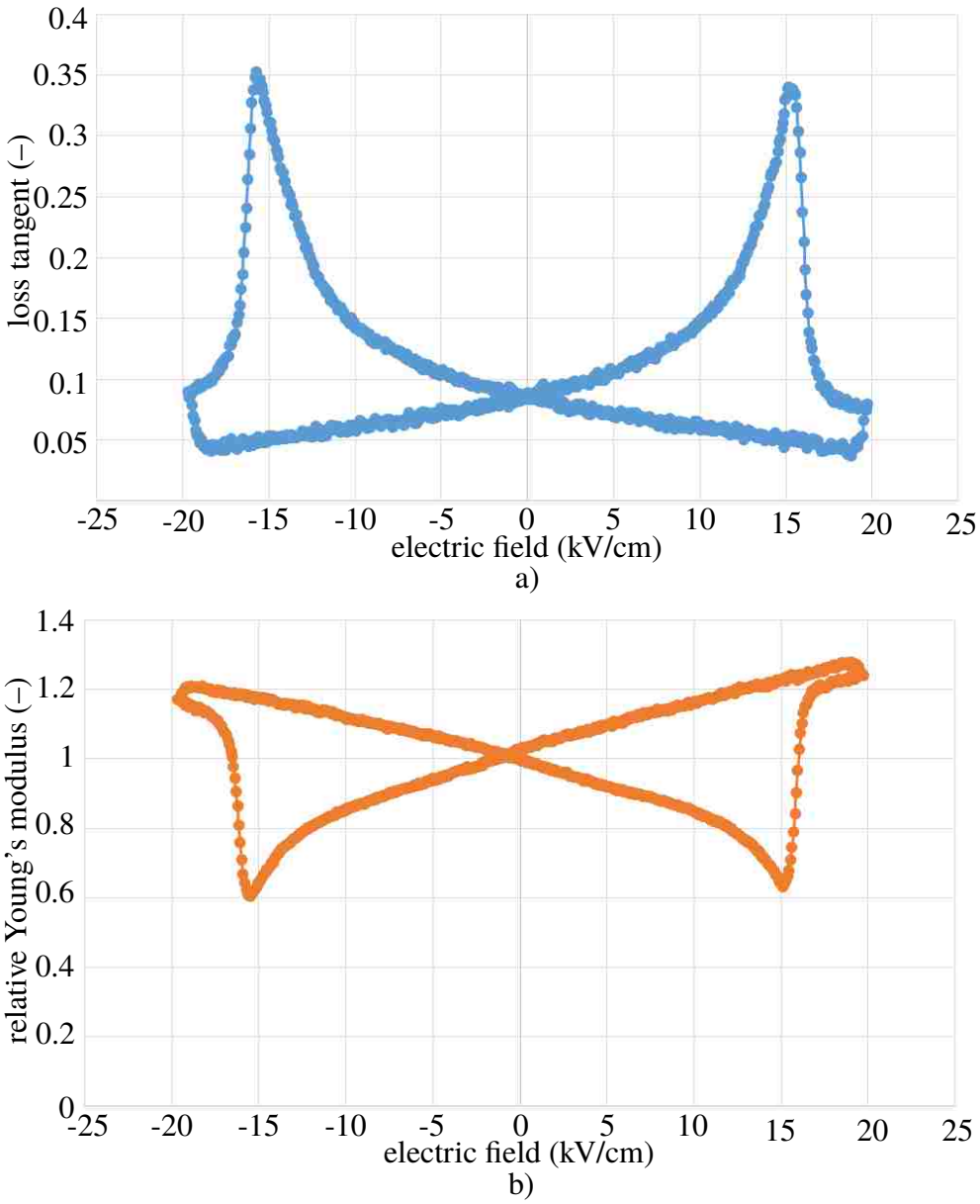

Figure 3.4. a) Loss tangent and b) relative Young's modulus vs. applied electric field for PZT-5A4E at a 75Hz mechanical load.

3.3. EXPERIMENTS AT CRYOGENIC TEMPERATURES

The temperature dependence of electric displacement, dynamic Young's modulus and loss tangent were measured utilizing the temperature control capabilities of the CBES. Tests on PZT specimens range in temperature from 34 K to 298 K, and therefore add to currently available experimental data on the effects of domain wall motion on the dynamic mechanical properties of ferroelectric ceramics.

3.3.1. P-E Curves at Different Temperatures. Following the methods used in measuring the P-E curves at room temperature, the electric displacement was measured for temperatures of 34 K (−240 °C), 73 K (−200 °C), 123 K (−150 °C), 173 K (−100 °C), and 223K (−50 °C). As shown in Figure 3.5, the spontaneous polarization and hysteretic affect significantly decrease as the temperatures reach cryogenic levels which is expected from literature [30].

As the temperature decreases, the spontaneous polarization in the positive direction decreases from 0.31 C/m^2 at 298 K, to 0.246 C/m^2 at 223 K, to 0.096 C/m^2 at 173 K, to a minimum value of 0.007 C/m^2 at 34 K. Furthermore, as the temperature decreases the coercive field first increases from 14 kV/cm at 298 K to 16 kV/cm at 223 K, then begins to decline to 11 kV/cm at 173 K, and continues to decrease as the temperature decreases. As both the spontaneous polarization and coercive field tend to lower values with decreasing temperature (at a sufficiently low temperature), the amount of domain switching also decreases. Thus, applications that seek to utilize domain switching at cryogenic temperature must account for this reduction of domain wall motion.

One can observe a difference between the electric displacement with respect to the sign of the applied electric field, as observable by the rounded corner of the P-E curve, at 223 K, during the maximum negative applied electric field. This artifact can be attributed to the pre-poling of the PZT specimens, such that the specimens are biased towards a particular polarization direction, and thus the spontaneous polarization and coercive fields

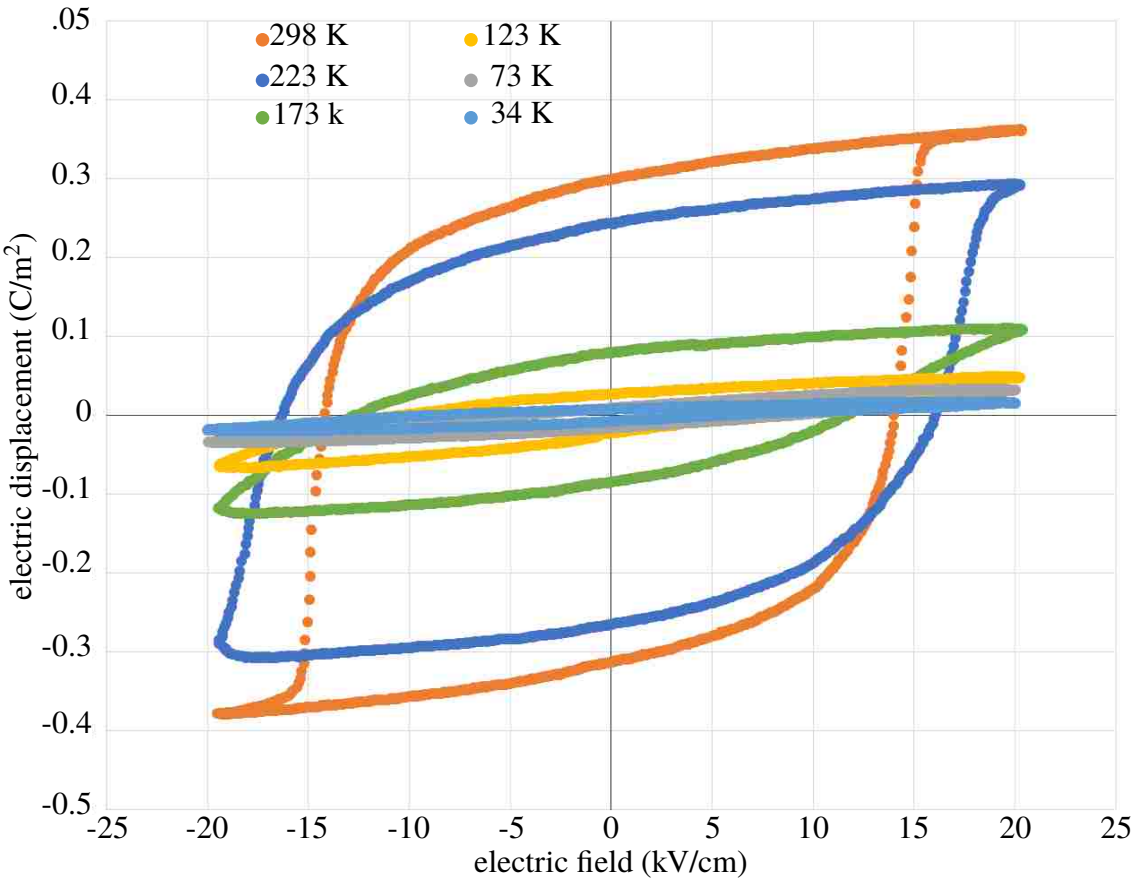

Figure 3.5. Temperature dependence of the P-E curves of PZT-5A4E for a frequency of an applied electric field of 50 mHz.

are direction dependent. As seen in the P-E curve for 223 K the spontaneous polarization is greater in magnitude in the negative direction (0.273 C/m^2) as compared to the positive direction (0.246 C/m^2).

It should be noted that as the electric field was cycled the temperature of the specimen increases. This temperature increase was greatest at the lowest temperature, 34 K, at which the temperature, as measured on the grips at base of the specimen, changed 6.8 K over 400 s during continuous cycling at an applied electric field frequency of 50 mHz. To avoid

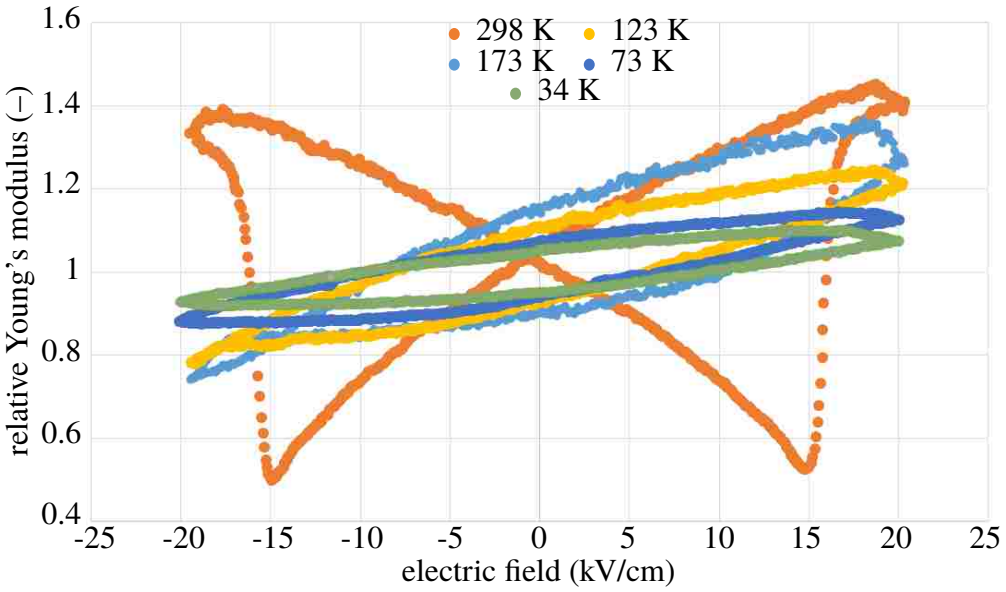

Figure 3.6. Relative Young's modulus measured at 298 K, 173 K, 123 K, 73 K and 34 K for a mechanical frequency of 100 Hz, and electric frequency of 50 mHz.

extreme temperature variances during testing, all measurements were taken within the first 40 seconds of applying the electric field. Between tests the specimen was allowed to reach and maintain the desired temperature for 10 minutes before a test was performed.

3.3.2. Dynamic Mechanical Properties of PZT at Different Temperatures. The dynamic Young's modulus and loss tangent of PZT-5A4E were measured while applied a cyclic electric field for a range of temperatures. As shown in Figure 3.7 and 3.6 the loss tangent and relative Young's modulus were measured at temperatures ranging from 34 K to 298 K. As before, all measurements were taken concurrently and the dynamic properties are reported versus the applied electric field.

As the temperature cools to the cryogenic range, the fluctuation of the Young's modulus with respect to the applied electric field is reduced. Below 173 K the relative Young's modulus becomes approximately linear with respect to the applied electric field, and proportional to the electric displacement (as shown in Appendix B). This demonstrates the dynamic Young's modulus at low temperatures tends towards a static Young's modulus,

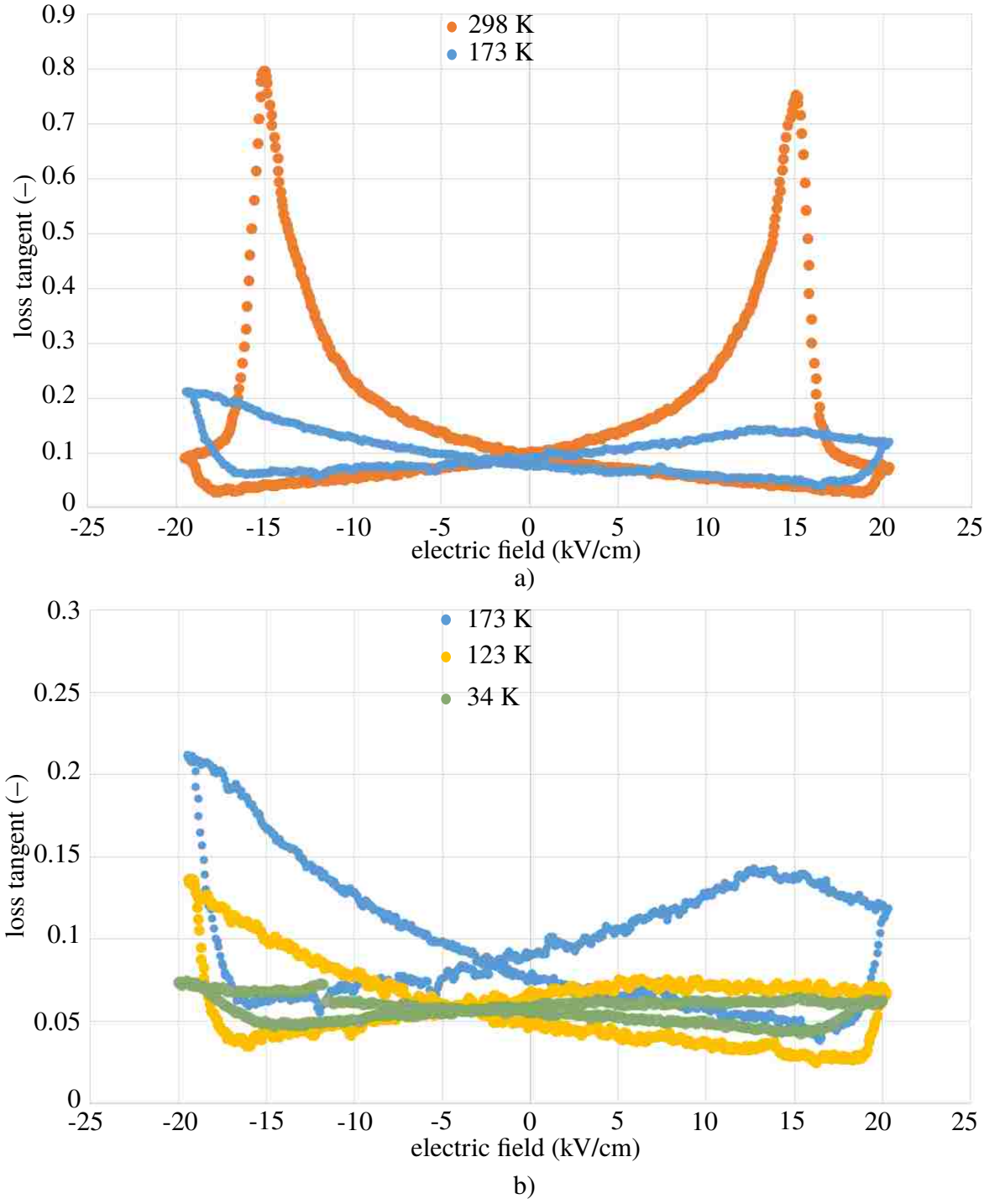

Figure 3.7. Loss tangent measured at a) 298 K and 173 K and b) 173 K, 123 K and 34 K for a mechanical frequency of 100 Hz, and electric frequency of 50 mHz. The loss tangent at 173 K is shown twice to allow for observation of the scale difference.

and that the relatively small change in the polarization of the PZT contributes to the small change Young's modulus. The dynamic mechanical properties of viscoelastic materials are generally known to be temperature dependent. In this case, the resulting loss tangent did not vary monotonically with temperature. The magnitude of the loss tangent, with respect to the applied electric field, shifted, such that at low temperatures the loss tangent no longer peaked before the maximum electric field is applied, instead the loss tangent increased approximately linearly until the maximum electric field was applied. After the peak of the electric field, the loss tangent decays back to the linear trend. However this decay is not consistent with measurements at higher temperatures, and was therefore not expected (for results from each temperature studied, see Appendix B). An additional experiment was performed in order to better understand what was affecting the loss tangent. Instead of applying a triangle wave electric field, a ramp-and-hold electric field was applied. In this test the electric field was ramped to the maximum field of the original triangle wave field (20 kV/cm) over 2.5 s. The maximum electric field was held for 5 s, then ramped in the opposite direction to the maximum (negative) field and held for 5 s. The test was carried out at 173 K as this was the temperature which best highlighted the peculiar loss tangent behavior in question. As shown in Figure 3.8, the loss tangent peaks and decreases prior to the maximum positive electric field, and only decreases when the negative applied electric field reaches its maximum and is held. This is comparable to the triangle wave test (Figure 3.7) where the loss tangent also peaks before the positive applied electric field, but does not peak until the maximum negative field is applied. One can also observe that the magnitude of the loss tangent does not reach as large of a value when the applied electric field is positive as compared to a negative applied electric field. The difference between the values and trend of the loss tangent with respect to the positive and negative applied electric field could be attributed to the pre-poling of the PZT specimens: a trend similar to that observed in the electric displacement, as shown previously in Figure 3.5.

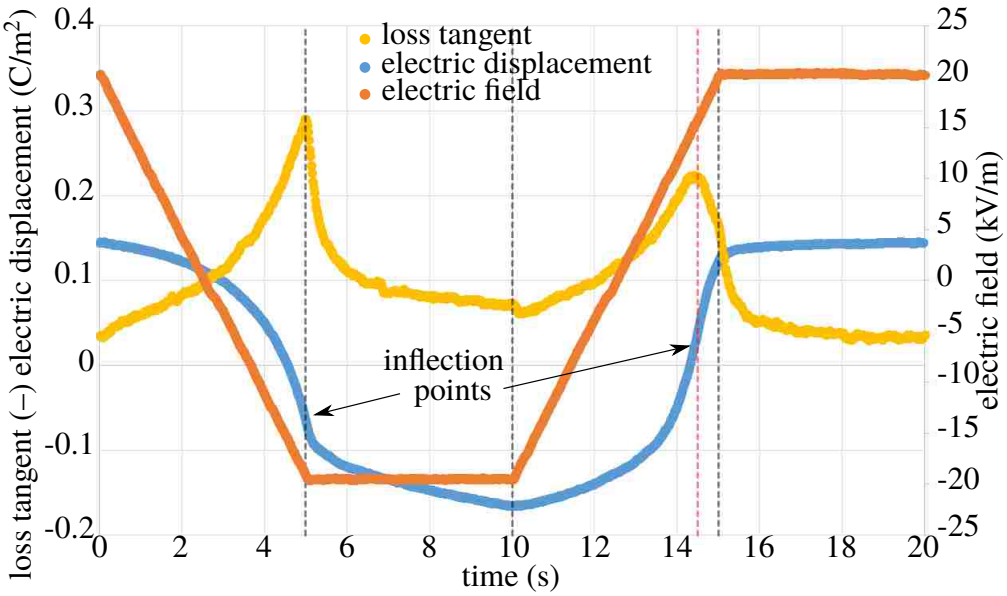

Figure 3.8. Ramp-and-hold electromechanical measurements for a mechanical frequency of 100 Hz at 173 K.

The electric displacement for the ramp-and-hold test was also plotted in Figure 3.8. It is important to note during the ramp-and-hold tests, the electric displacement continues to increase in magnitude after the maximum negative electric field has been reached and held, and does not begin to decrease until the applied electric field begins to change. This could be due to a temperature dependence of domain wall motion, such that as the temperature decreases the speed of domain wall motion is decreased and therefore, as shown in Figure 3.8, the total polarization of a bulk specimen is slower to increase in magnitude. This same behavior is observed at room temperature at high electric field frequencies where the domain wall motion is too slow to respond to the rapidly changing electric field [84]. This is a possible explanation for the continued change of electric displacement as the applied electric field was held constant. Another observation is the relationship between the electric displacement inflection points and the loss tangent peaks. This shows a potential correlation between the loss tangent and the time rate of change of polarization, or a relationship between domain wall velocity and loss tangent. To better demonstrate this,

the loss tangent was plotted with respect to the rate of change of the electric displacement, and is shown in Figure 3.9. Since the loss tangent is physically due to internal dissipation mechanisms in the material, in this case domain switching, the loss tangent should be related to the rate of change of the overall electric displacement. As temperature affects domain wall motion, it follows that temperature will also affect the rate of change of the electric displacement.

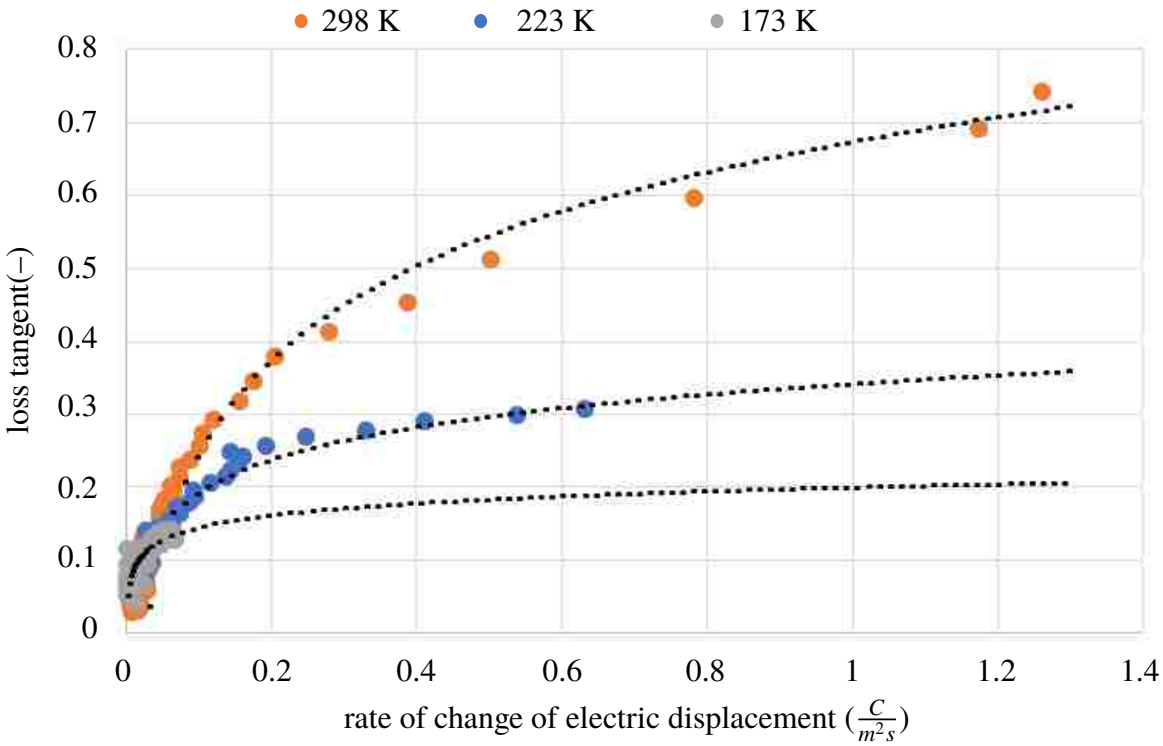

Figure 3.9. Loss tangent plotted against the rate of change of electric displacement for PZT at temperatures of 298 K, 223 K and 173 K for a mechanical frequency of 100 Hz and electrical frequency of 50 mHz.

The temperature dependence of the rate of change of polarization permits a specimen at higher temperatures to achieve a larger value of $\Delta P/\Delta t$. This is expected since it has been previously suggested that the rate of change of polarization is dependent on both temperature and applied electric field [57]. From Figure 3.9 we can determine the relationship between the loss tangent and the time rate of change of polarization, which is well fit by a natural log curve. The equations for the trend-lines from Figure 3.9 at the temperatures of 298 K,

223 K, and 173 K are

$$\tan \delta_{298} = 0.185 \ln \frac{\Delta P}{\Delta t} + 0.676, \tag{3.2}$$

$$\tan \delta_{223} = 0.06452 \ln \frac{\Delta P}{\Delta t} + 0.3428, \tag{3.3}$$

and

$$\tan \delta_{173} = 0.0238 \ln \frac{\Delta P}{\Delta t} + 0.2008, \tag{3.4}$$

respectively.

4. CONCLUSION AND FUTURE WORK

By designing and building the novel CBES setup, the goal of closing the gap in experimental capabilities was achieved. CBES enables the temperature controlled dynamic electromechanical testing of bulk ferroelectric ceramics, due to its capability to individually or concurrently measure the dynamic mechanical and electrical properties in cryogenic temperatures. The test specimens can have a modulus up to 10^4 GPa and be tested through a frequency range from 10^{-1} to 10^4 Hz. The CBES can also test electrical properties under an applied electric field up to 200 kV/m at a frequency of up to 7.5 kHz. The influence of temperature can be measured from 325 K to 34 K, and all tests can be performed under vacuum at a pressure of 4×10^{-7} mbar. The apparatus goes beyond current state of the art equipment and allows for measuring material properties in a simulated space environment. Validation of the the measurement capabilities of the CBES setup show the accuracy of the instrumentation. New results have been reported, providing insight to the dependence of dynamic mechanical properties on both the rate of change of polarization, and temperature. In particular, the experiments have revealed a relationship between domain wall velocity and loss tangent. While this is dependence is expected [82, 1], the exact relationship between damping and domain wall motion is still not well understood. The CBES allows provides a means to gain insight into this relationship. Such knowledge will aid in the design of improved ferroelectric material microstructures and compositions with improved properties. Due to the equipment being designed such that it is capable of measuring material properties over a broad spectrum of loading scenarios, there are many possibilities for future work with the CBES. To this end a list of potential studies utilizing the testing capabilities are described as follows.

1. Testing different ferroelectric materials: Through the creation validation and initial study of the CBES only PZT 5A4E was tested to the full extent of the capabilities of the CBES. As mentioned previously there are a multitude of different ferroelectric materials, both ceramics and polymers. These other materials, (e.g. barium titanate, bismuth titanate, europium barium titanate, germanium telluride, lead scandium tantalate, lead titanate, lithium niobate, polyvinylidene fluoride, potassium niobate, and potassium titanyl phosphate) are able to be tested at cryogenic temperatures. While some properties, such as the electric or mechanical properties, of these materials have been tested at low temperatures, the dynamic mechanical properties during domain switching have not. This setup allows for the testing of a wide range of materials, and a possible future research direction is to characterize other ferroelectric materials. The CBES also allows for non-ferroelectric materials to be tested for viscoelastic properties over the 34-300 K temperature range.

2. Testing different compositions of PZT: The composition of the PZT which was tested in this study is shown in Table 3.1. This material composition of PZT falls into the range highlighted in yellow in Figure 4.1. However to study the properties of materials with different phases or a material going through a phase transition one could have a PZT with a titanium composition of 0.4-0.6 in the range of the blue highlighted region which allows for temperature dependent phase transitions. The ability to study different phases of material allows for the characterization of phase dependent properties such as electromechanical coupling. Also phase boundaries such as the morphotropic phase boundary (MPB in Figure 4.1), can exhibit properties such as a giant dielectric response and high electromechanical coupling [32].

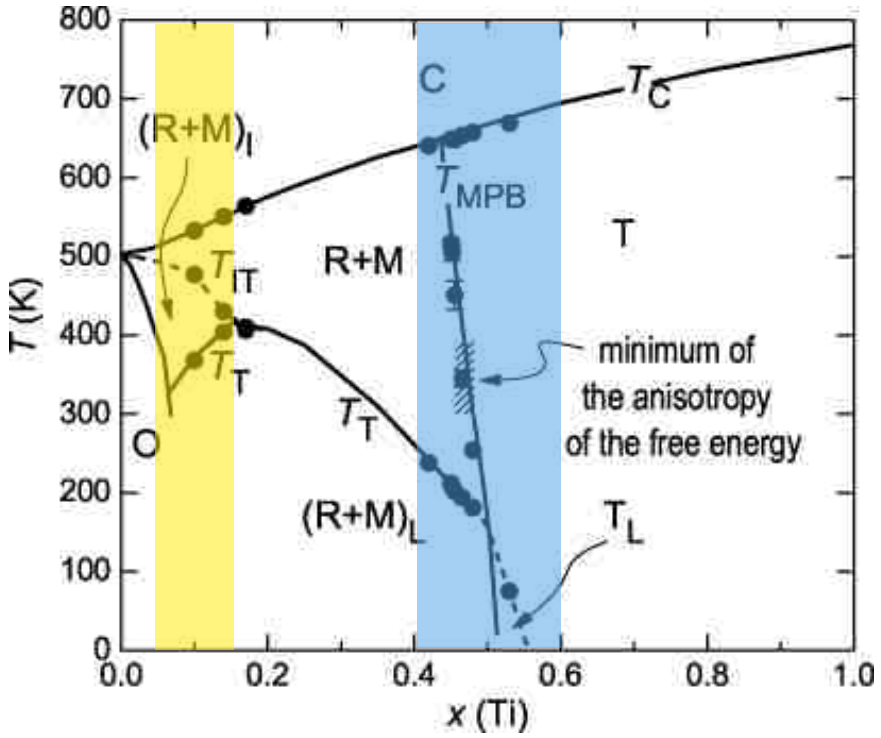

Figure 4.1. Phase diagram for PZT [14], with the yellow area denoting the composition of the PZT tested in this study, and the blue area denoting the recommended composition for future testing.

3. Influence of electric field frequency: This study focused on the dynamic mechanical properties during domain switching, and shows the relationship between the loss tangent and the rate of change of polarization. To this end, a possible next step in characterizing the loss tangent with respect to the rate of change of polarization is to apply the electric fields at different frequencies. In this way, the magnitude of the polarization change could be increased and the relationship between the loss tangent and rate of change of polarization could be extended. The current known limit to the ability to perform this test resides in the high voltage amplifier. During previous studies, the electrical cycling rate was limited to 5 Hz because at that rate the current draw from the high voltage amplifier exceeded the rating of the equipment. This current draw will decrease at lower temperatures but to do higher frequency testing it may be necessary to use a high voltage amplifier with a larger current output rating.

4. Heat generation due to electric cycling: It is known that ferroelectrics produce heat when a sufficiently large electric field is applied and understanding the heat generation of materials to be used in temperature sensitive environments is critical. The CBES currently measured a temperature gain during the electromechanical testing, but this was not the goal of this study. The CBES has ability to measure the temperature change (and thus the heat generation) of PZT at different initial temperatures, magnitudes of applied electric fields, and frequencies of applied electric fields. A study similar to this has been completed for PZT using the CBES by Wiebe Boleij under the advisement of Dr. Charles Wojnar, to characterize the heat generation at room temperature. However this study can be continued by testing over the temperature range of the CBES.

5. Fatigue and aging: The CBES allows for extended testing under thermal, electrical and mechanical loads. This allows for fatigue and aging tests to be completed in one system without the need to remove, replace, or adjust the specimen being tested. Fatigue in ferroelectrics is not just in the mechanical sense, to be measured over a number of loading cycles, but also includes electrical fatigue, in which the specimen is loaded by a cyclically applied electric field, leading to polarization degradation. This is currently studied separately, either the mechanical or electrical fatigue being the focus. The CBES allows for the simultaneous study of mechanical and electrical loading and thus the simultaneous study of mechanical and electrical fatigue. Aging, is the change in either mechanical or electrical properties over time without external applied loads. Similarly the aging of ferroelectrics is currently studied individually, with the CBES allowing for the simultaneous study of aging on electrical and mechanical properties. The CBES also allows for the temperature dependence of both fatigue and aging studies to be measured. Non-ferroelectric materials can also be tested for fatigue and aging in the CBES, e.g. solid rocket propellant.

6. Ferroelectric set-and-hold actuation: As proposed by Wojnar [74], set-and-hold actuation utilizing domain switching in ferroelectrics could be used as a semi-active method for controlling displacement. This actuation utilizes the strain induced in a ferroelectric by applying a coercive field to realign the domain orientations. This allows for a one time activation of the actuator which will deform and remain deformed until a coercive field is applied in a different direction. Some proposed applications of these are for aerospace applications, specifically for space telescopes. Previously, the proof of concept testing of set-and-hold actuators was performed at room temperature. However for the proposed application, the proof of concept should be evaluated in the true application setting. To this end the CBES allows for the testing of these actuators such as micro fiber composites (MFC's) as used by Wojnar [74], in the intended use environment, i.e. at cryogenic temperatures in a vacuum environment. The CBES could also be used with a digital image correlation set-up allowing for the strain of the actuator, or specimen to be measured over the temperature range.

7. Implementation of different specimen testing fixtures: The CBES is robust in design and allows for modular testing set-ups to replace the electrical isolating grips and Helmholtz coils. With this, the CBES allows for any testing apparatus needing up to 20 standard (non-high voltage) electrical connections, up to 4 high voltage electrical connections, optical line of sight for a setup 5" in height and the setup must fit within a 3.545" radius area and volume of less than 266.5 in^3. Thus, it is possible to run uniaxial tensile or compression tests for materials with or without application of electric fields, or it is possible to implement an impact, displacement, or fracture testing setup.

APPENDIX A

PICTURES OF CBES SETUP

The solid model and schematics of the CBES setup are shown in the above report. The appendix contains pictures of the equipment in the setting in which it was used. An important note is that the Young's modulus will be reported as relative Young's modulus such that comparisons can be made to literature [75, 39, 74]. This relative Young's modulus is the measure of the instantaneous amplitude of deflection with no applied electric field u_z^0 over the amplitude of the deflection when a field is applied u_z, as shown by

$$\frac{E}{E^0} = \frac{u_z^0}{u_z}, \tag{A.1}$$

where the E is the dynamic Young's modulus and E^0 is the dynamic Young's modulus with no applied electric field.

PICTURES OF THE CBES AND ANCILLARY EQUIPMENT

The CBES, in the open (specimen accessible) position and closed (operating) position are shown in Figures A.1 and A.2, respectively. With Figure A.3 showing the Helmholtz coils and specimen setup. Figures A.4, A.5, and A.6 show the temperature controller, vacuum pumping station, and cryo-pumping station, respectively. All other ancillary electrical equipment is housed in an electronics rack as shown by Figure A.7

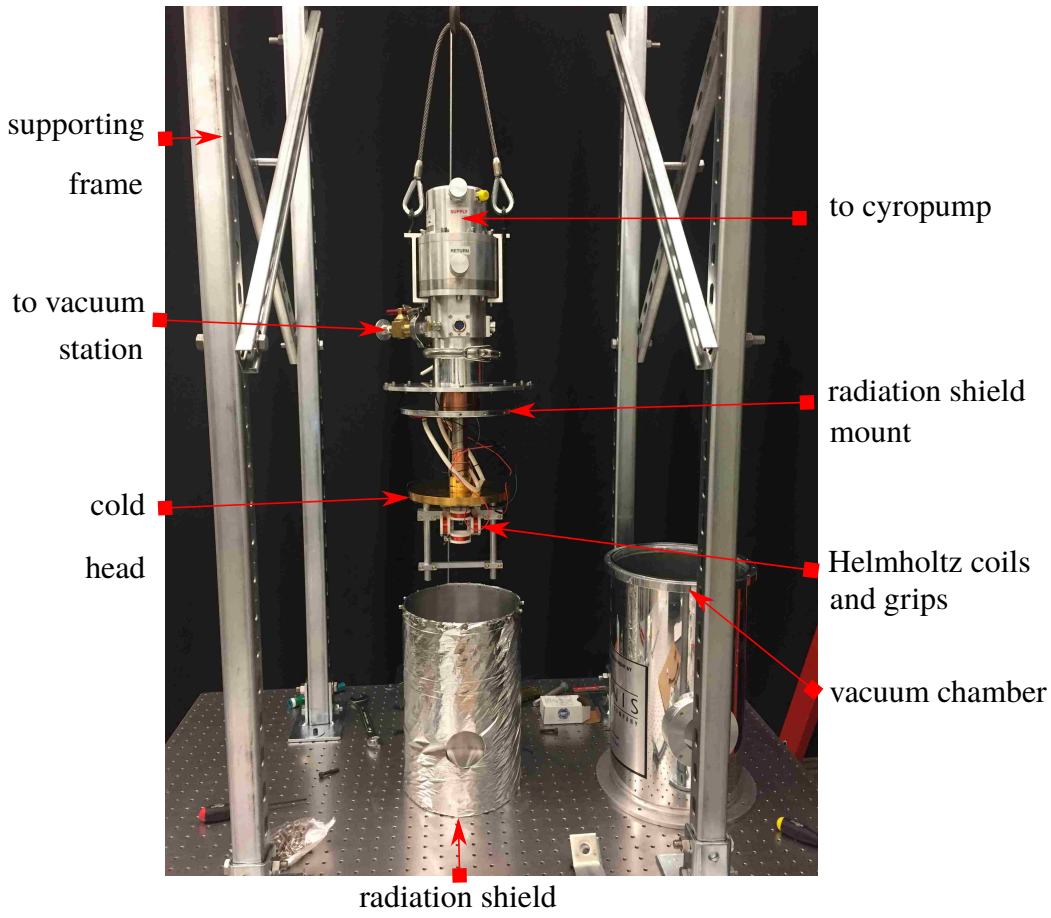

Figure A.1. Picture of the CBES while in the open position allowing for access to the specimen, magnet clamp, Helmholtz coils and temperature sensors.

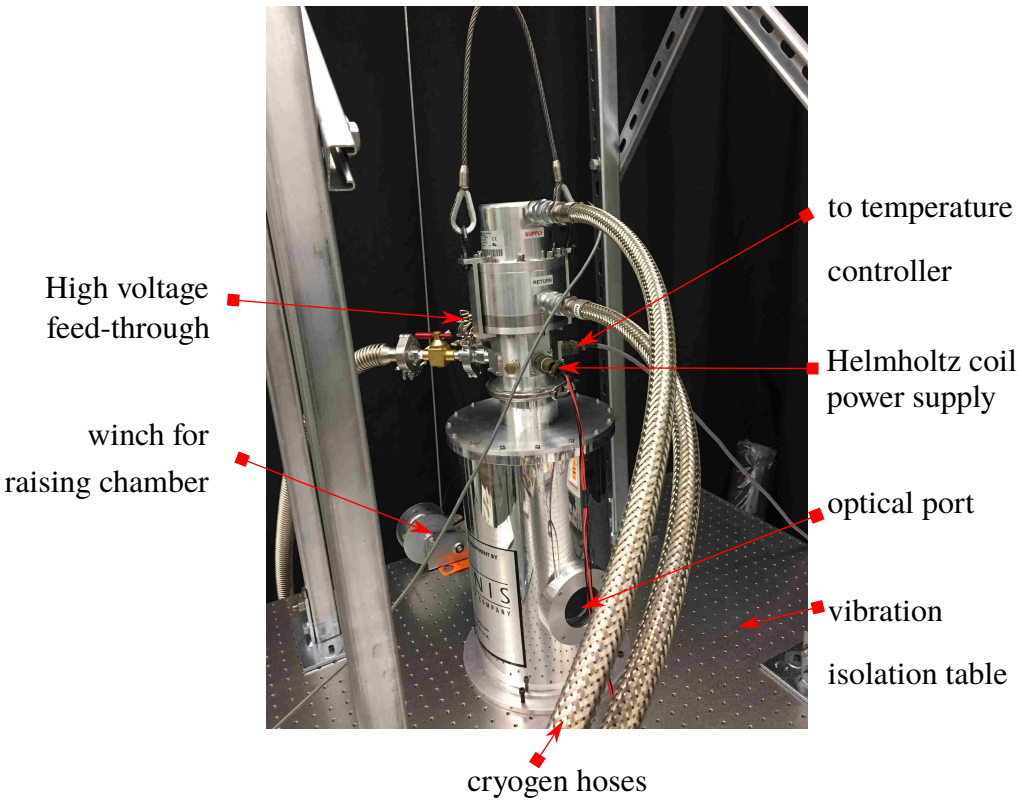

Figure A.2. Picture of the CBES in the closed position, allowing for the operation of the CBES.

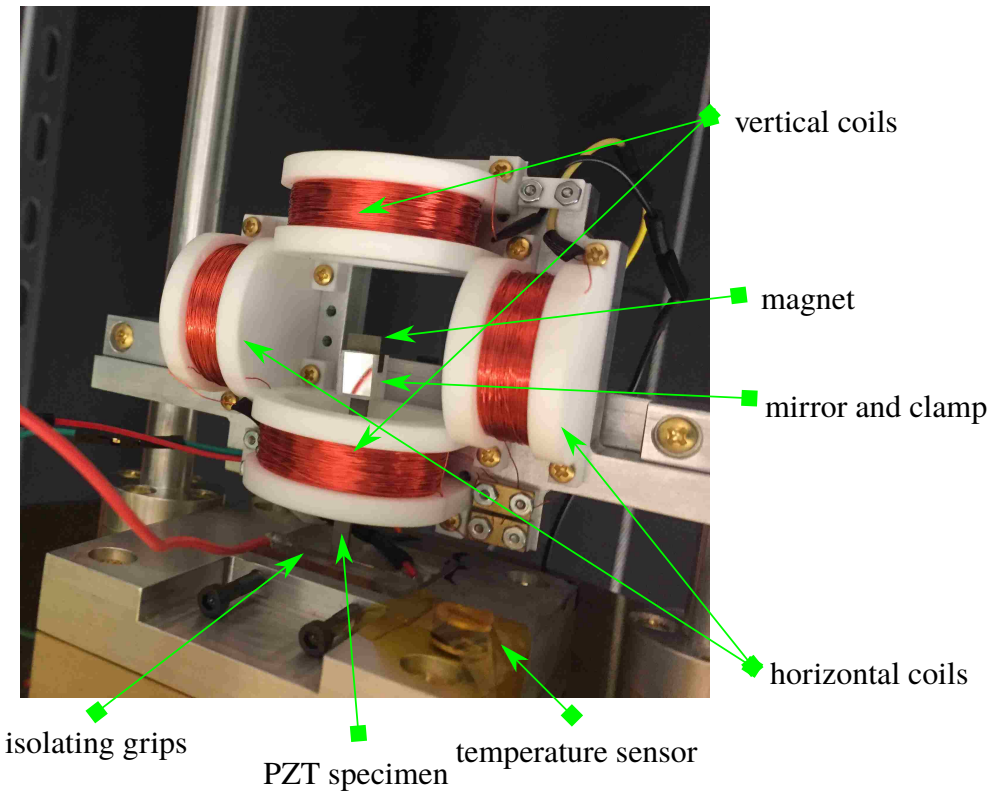

Figure A.3. A close up view of the Helmholtz coils, specimen, magnet and mirror clamp, and temperature sensor.

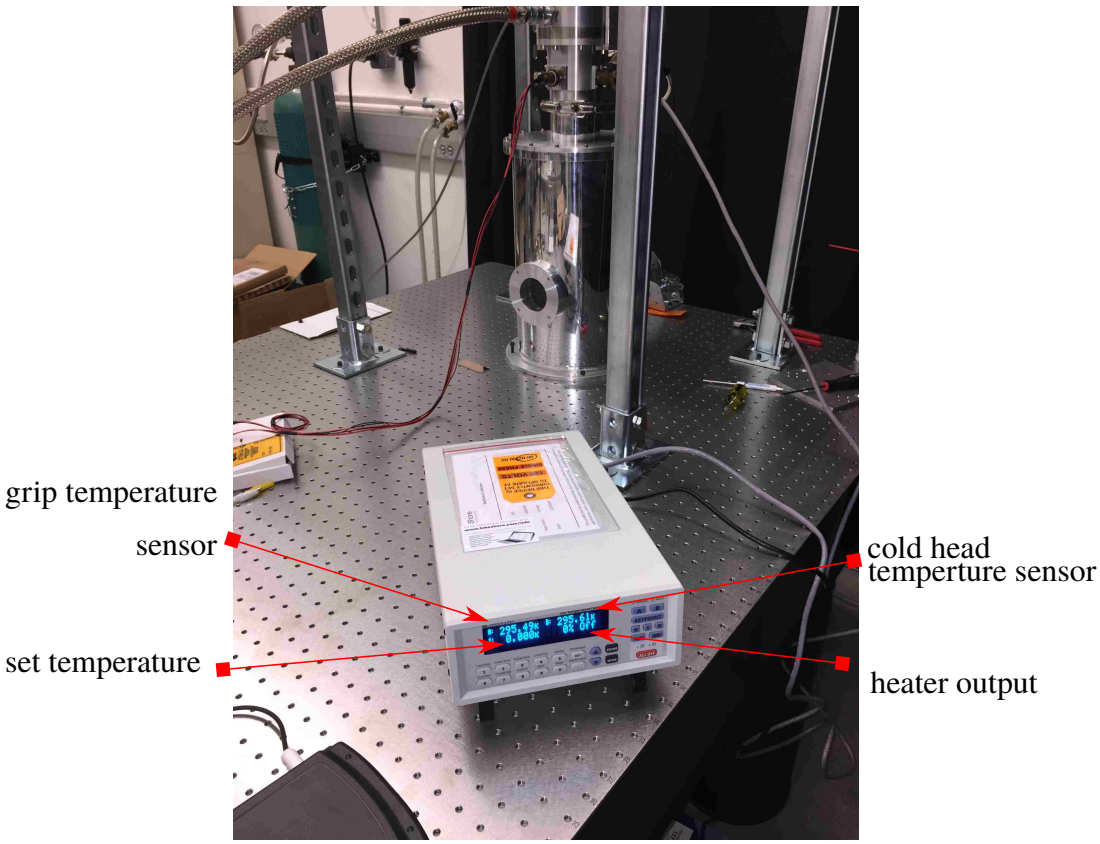

Figure A.4. Lakeshore Model 335 temperature controller used in the CBES.

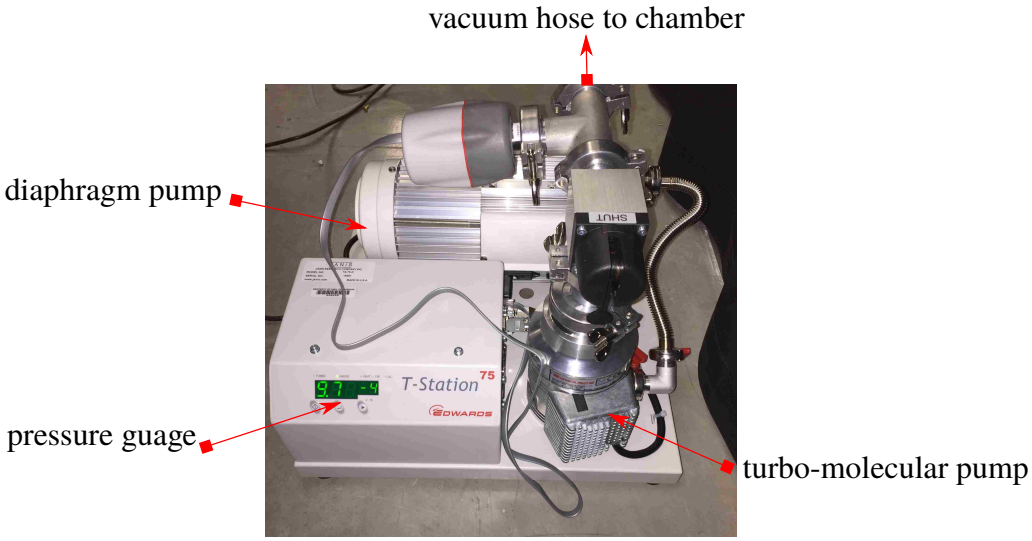

Figure A.5. Picture of the Edwards T-Station 75 vacuum pumping station.

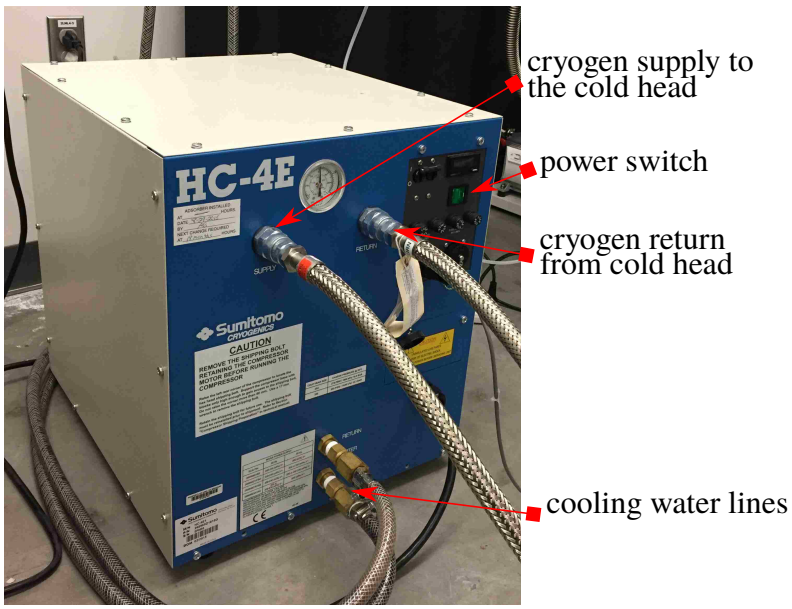

Figure A.6. The Sumitomo HC-4E1 cryopump used in the CBES set-up.

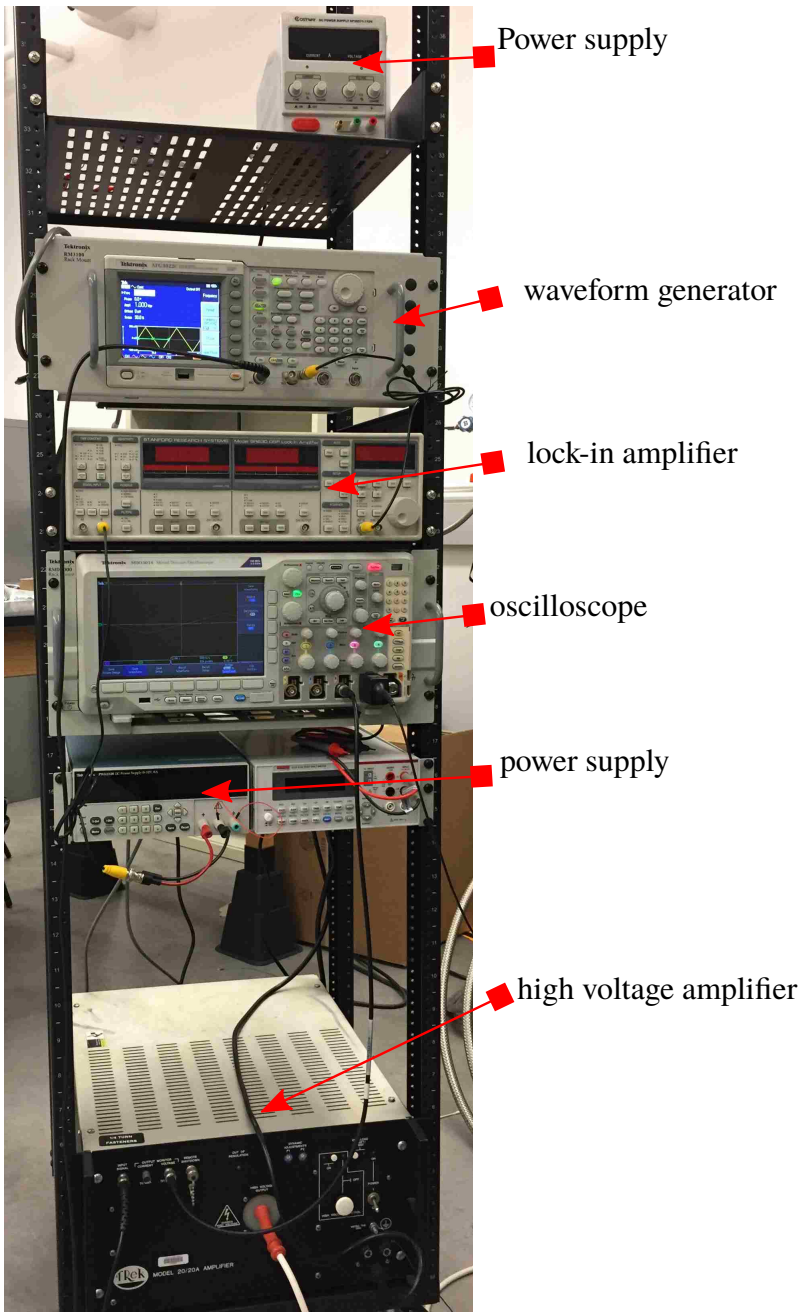

Figure A.7. The electronics rack containing two DC power supplies (Tektronix PWS2300 and Yescom 30 V 5 A), TekTronix AFG3022c waveform generator, Tektronix MDO 3014 oscilloscope, and the Trek 20/20A high voltage amplifier.

DESIGN OF CURRENT ISOLATION CIRCUIT

The circuit shown in Figure A.8, was designed to be used with a voltage signal, as provided by the waveform generator, and two power supplies, one positive and one negative, as see in the electronics rack in Figure A.7. This circuit uses a LM358 op-amp in a standard voltage follower circuit, and uses a pair of TIP31 and TIP32 bipolar transistors to allow for the AC power to be provided by the DC power supplies.

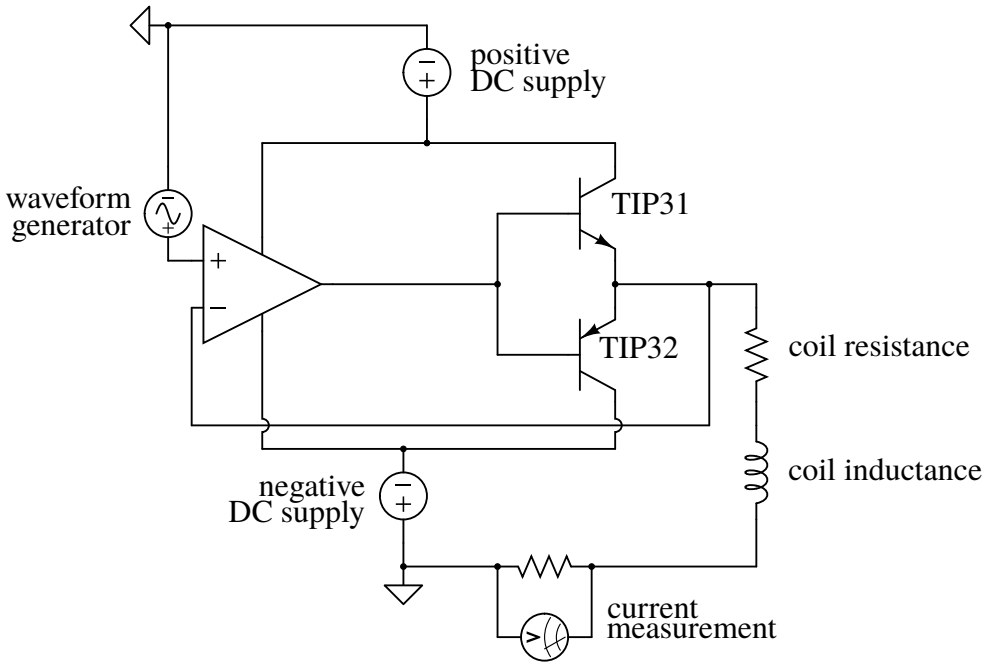

Figure A.8. Circuit diagram for the current isolation circuit used to amplify the power abel to be supplied to the Helmholtz coils.

APPENDIX B

CONCURRENT MEASUREMENTS FOR DIFFERENT TEMPERATURES

The CBES was used to study the temperature dependence of the dynamic mechanical properties during domain switching of PZT 5A4E. Separate plots of electric displacement, dynamic Young's modulus, and loss tangent were shown in previous figures. Here, the complete set of data obtained from the scope versus time is shown. In the following appendix, data collected from temperature ranges 73 K through 298 K are provided and the data for each measurement will be plotted against time. The temperatures are 298 K, 223 K, 173 K, 123 K, and 73 K

TESTING AT DIFFERENT TEMPERATURES

Figure B.1 and Figure B.2 show room temperature data for two different specimens, specimen A and specimen B, respectively.

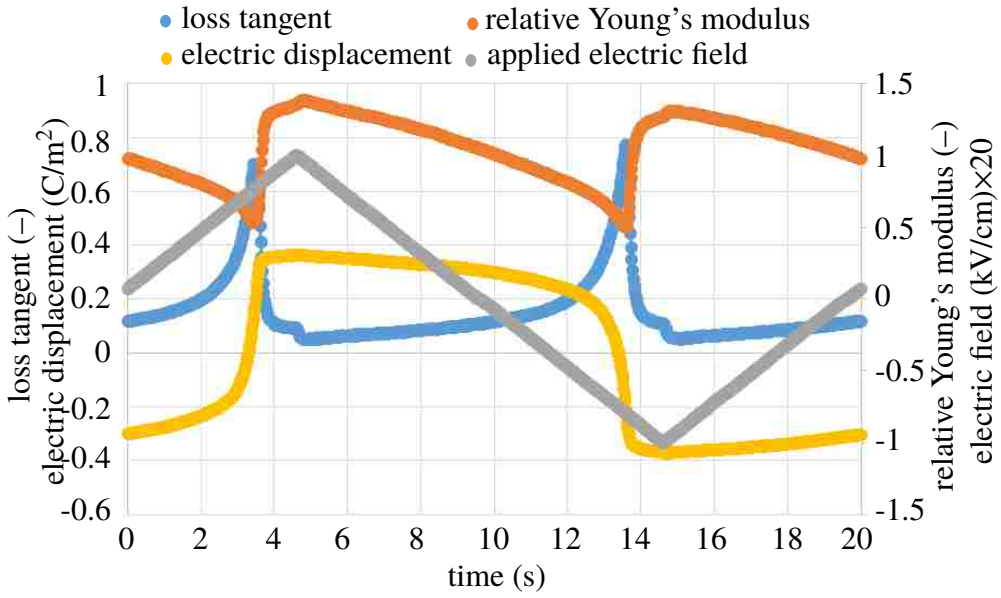

Figure B.1. Concurrent measurements at 298 K for specimen A, at a mechanical frequency of 100 Hz, and electrical frequency of 50 mHz

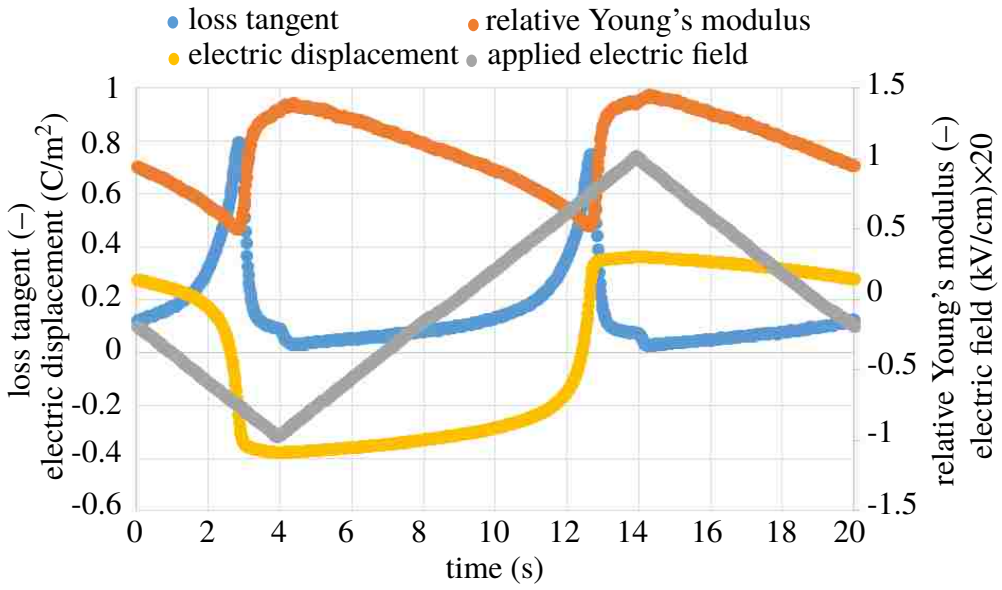

Figure B.2. Concurrent measurements at 298 K for specimen B, at a mechanical frequency of 100 Hz, and electrical frequency of 50 mHz

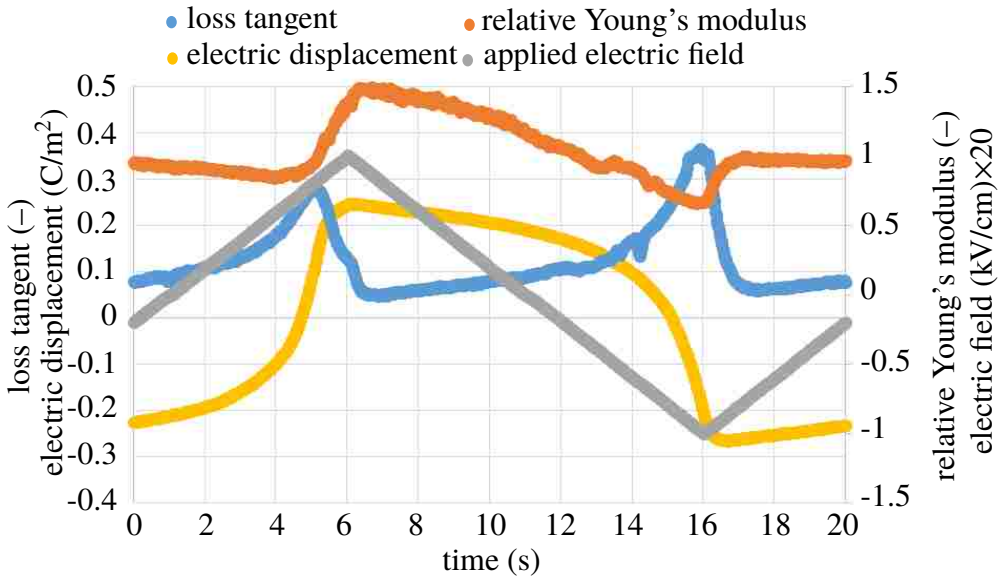

Figure B.3. Concurrent measurements at 223 K for specimen A, at a mechanical frequency of 100 Hz, and electrical frequency of 50 mHz

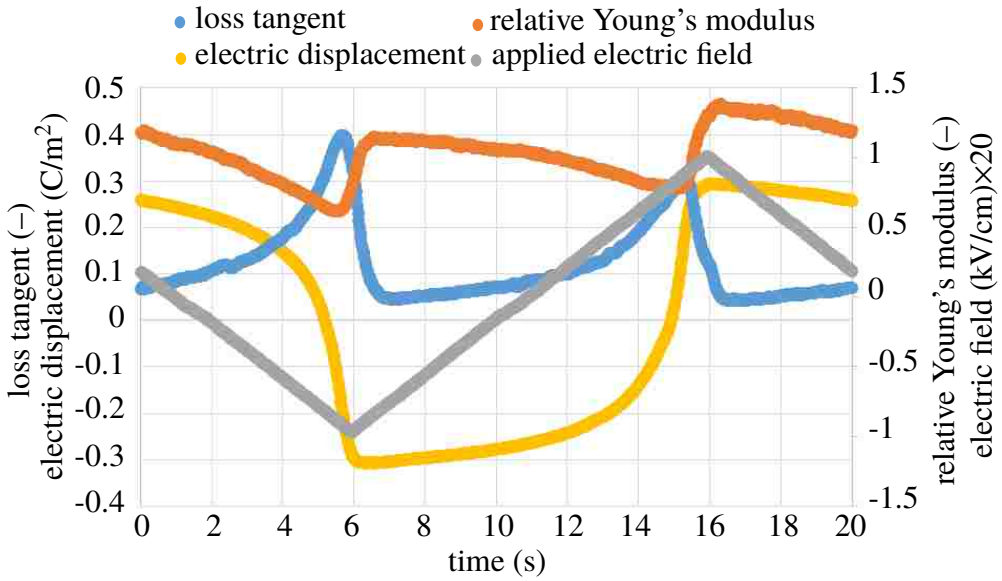

Figure B.4. Concurrent measurements at 223 K for specimen B, at a mechanical frequency of 100 Hz, and electrical frequency of 50 mHz

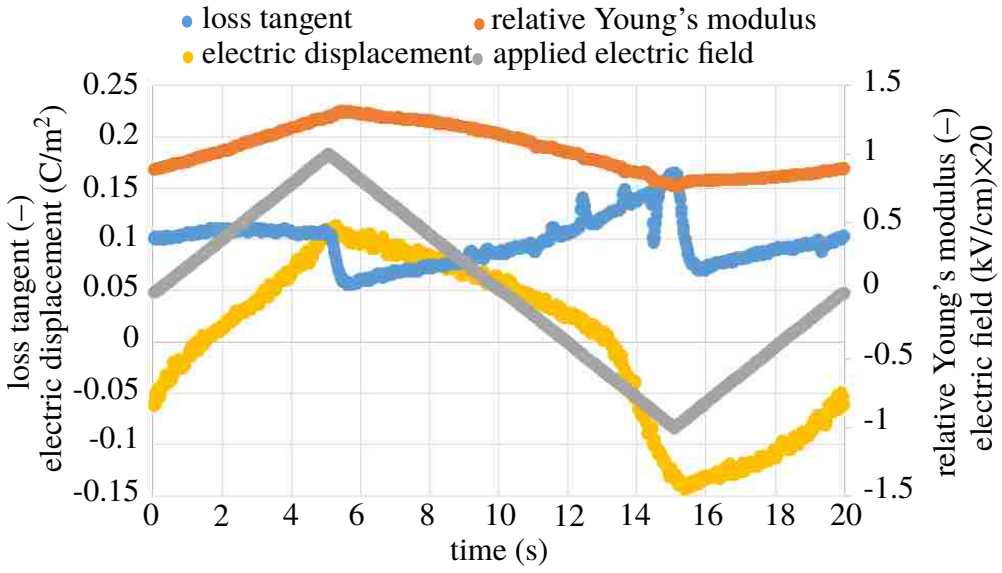

Figure B.5. Concurrent measurements at 173 K for specimen A, at a mechanical frequency of 100 Hz, and electrical frequency of 50 mHz

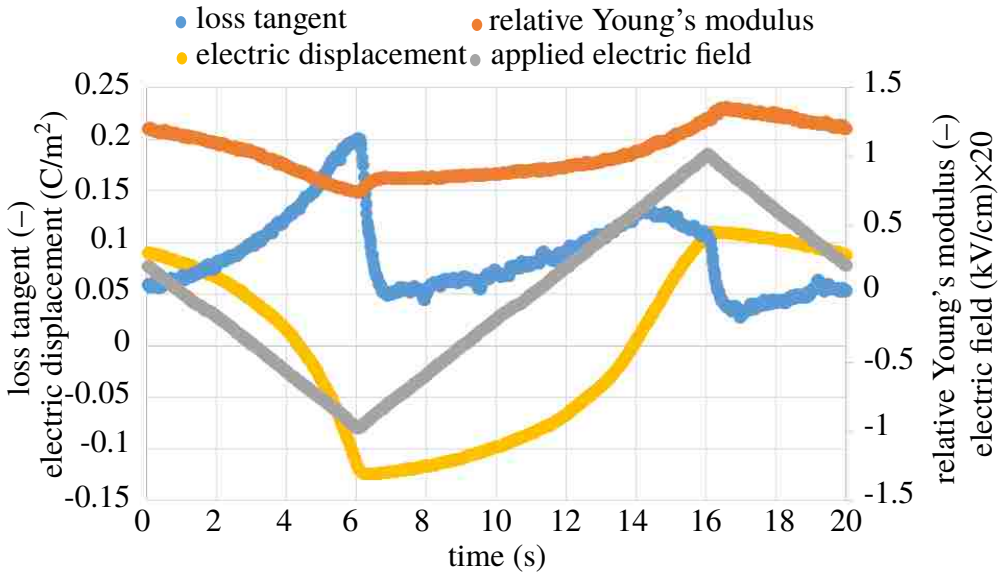

Figure B.6. Concurrent measurements at 173 K for specimen B, at a mechanical frequency of 100 Hz, and electrical frequency of 50 mHz

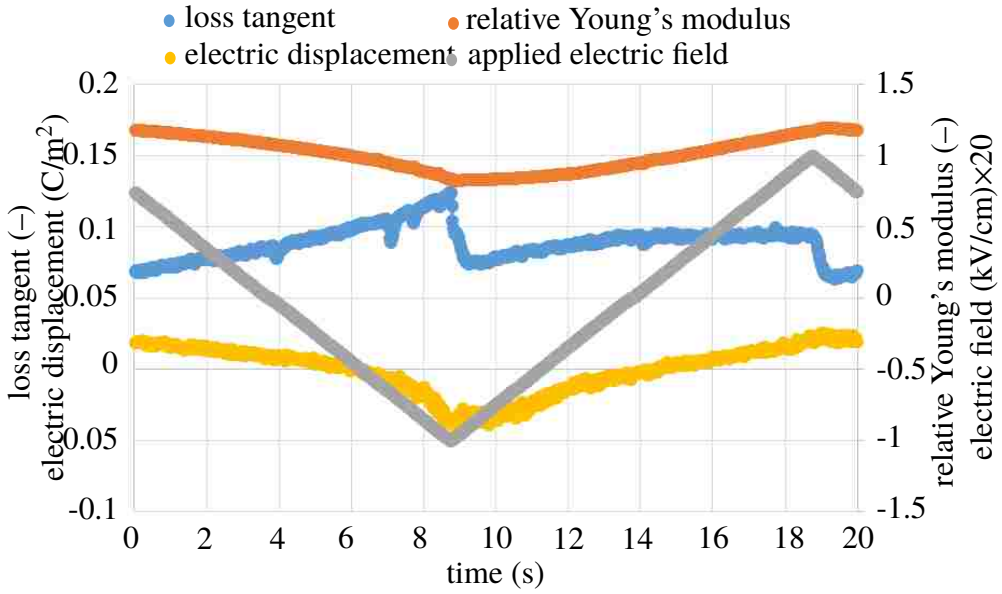

Figure B.7. Concurrent measurements at 123 K for specimen A, at a mechanical frequency of 100 Hz, and electrical frequency of 50 mHz

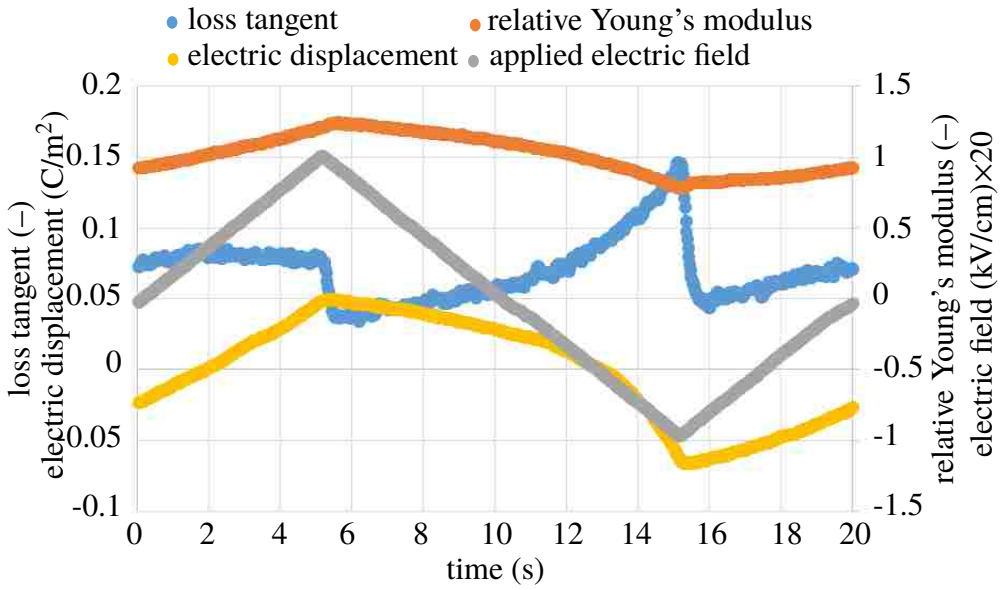

Figure B.8. Concurrent measurements at 123 K for specimen B, at a mechanical frequency of 100 Hz, and electrical frequency of 50 mHz

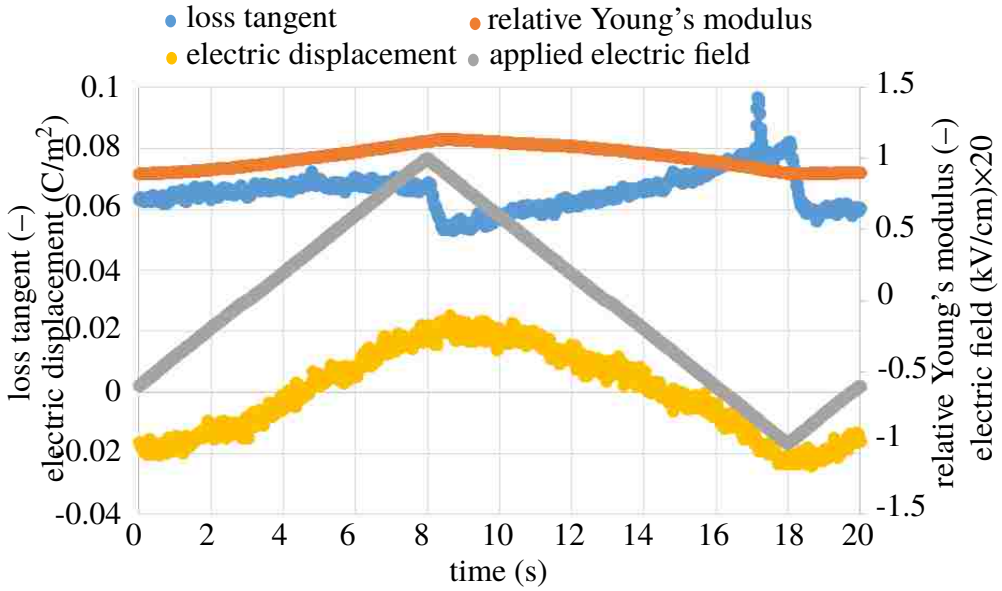

Figure B.9. Concurrent measurements at 73 K for specimen A, at a mechanical frequency of 100 Hz, and electrical frequency of 50 mHz

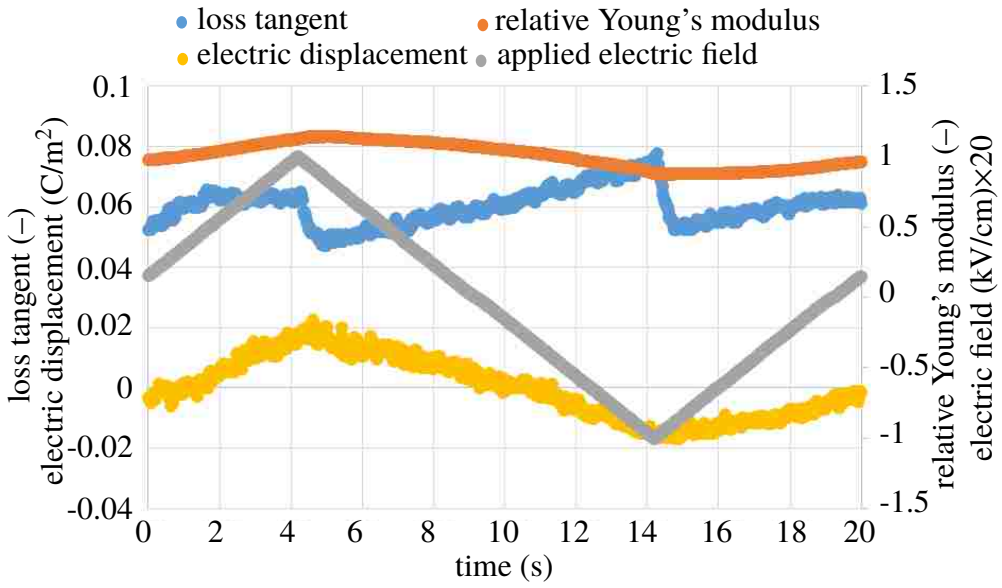

Figure B.10. Concurrent measurements at 73 K for specimen B, at a mechanical frequency of 100 Hz, and electrical frequency of 50 mHz

REFERENCES

[1] G. Arlt and H. Dederichs. Complex elastic, dielectric and piezoelectric constants by domain wall damping in ferroelectric ceramics. *Ferroelectrics*, 29(1):47–50, 1980. doi: 10.1080/00150198008009006. URL http://www.tandfonline.com/doi/abs/10.1080/00150198008009006.

[2] T. Asare. *Investigating Ferroelastic and Piezoelectric Vibration Damping Behavior in Nickel-Barium Titanate and Nickel-PZT Composites*. PhD thesis, Virginia Polytechnic Institute and State University, 2007.

[3] T. Asare, B. Poquette, J. Schultz, and S. Kampe. Investigating the vibration damping behavior of barium titanate (batio3) ceramics for use as a high damping reinforcement in metal matrix composites. *Journal of Materials Science*, 47 (6):2573–2582, 2012. ISSN 0022-2461. doi: 10.1007/s10853-011-6080-9. URL http://dx.doi.org/10.1007/s10853-011-6080-9.

[4] F. Bachmann, R. de Oliveira, A. Sigg, V. Schnyder, T. Delpero, R. Jaehne, A. Bergamini, V. Michaud, and P. Ermanni. Passive damping of composite blades using embedded piezoelectric modules or shape memory alloy wires: a comparative study. *Smart Materials and Structures*, 21(7):075027, jun 2012. doi: 10.1088/0964-1726/21/7/075027.

[5] D. Brewster. *Observations of the pyro-electricity of minerals*, volume 2, chapter Art. II, pages 208–215. The Edinburgh Journal of Science, 1824.

[6] F. Y. Bruno, S. Boyn, S. Fusil, S. Girod, C. Carrétéro, M. Marinova, A. Gloter, S. Xavier, C. Deranlot, M. Bibes, A. Barthélémy, and V. Garcia. Millionfold resistance change in ferroelectric tunnel junctions based on nickelate electrodes. *Advanced Electronic Materials*, 2(3):1500245, jan 2016. doi: 10.1002/aelm.201500245.

[7] d. buck, massachusetts inst of tech cambridge digital computer lab., massachusetts institute of technology. digital computer laboratory, and project whirlwind. *Ferroelectrics for Digital Information Storage and Switching*. Report (Project Whirlwind). Defense Technical Information Center, 1952. URL https://books.google.com/books?id=ya0MHQAACAAJ.

[8] G. Carman and G. McKnight. Damping in composite materials through domain wall motion, 01 2002. patent.

[9] P. M. Chaplya and G. P. Carman. Compression of piezoelectric ceramic at constant electric field: Energy absorption through non-180° domain-wall motion. *Journal of Applied Physics*, 92(3):1504–1510, 2002. doi: 10.1063/1.1489498. URL http://link.aip.org/link/?JAP/92/1504/1.

[10] C. H. Chen, Y. Y. Lin, Y. C. Wang, W. L. Huang, and N. L. Shih. Damping induced from the interaction between a vibrating cantilever and its surroundings. *Advanced Materials Research*, 787:798–802, sep 2013. doi: 10.4028/www.scientific.net/amr.787.798.

[11] L. Chen, Z. Cheng, W. Xu, X. Meng, G. Yuan, J. Liu, and Z. Liu. Electrical and mechanical switching of ferroelectric polarization in the 70 nm BiFeO3 film. *Scientific Reports*, 6(1), jan 2016. doi: 10.1038/srep19092.

[12] L. Cheng, B., M. Gabbay, M. Maglione, Y. Jorand, and G. Fantozzi. Domain walls motions in barium titanate ceramics. *J. Phys. IV France*, 06(C8):C8–647–C8–650, 1996. URL http://dx.doi.org/10.1051/jp4:19968139.

[13] K. J. Choi. Enhancement of ferroelectricity in strained BaTiO3 thin films. *Science*, 306(5698):1005–1009, nov 2004. doi: 10.1126/science.1103218.

[14] F. Cordero, F. Trequattrini, F. Craciun, and C. Galassi. Octahedral tilting, monoclinic phase and the phase diagram of PZT. *Journal of Physics: Condensed Matter*, 23(41): 415901, sep 2011. doi: 10.1088/0953-8984/23/41/415901.

[15] J. Curie and P. Curie. Développement, par pression, de lâélectricité polaire dans les cristaux hémièdres à faces inclinées. *Comptes Rendus de lâAcadémie des Sciences*, 91:294âĂŞ295, 1880.

[16] D. DeTroye and R. Chase. The calculation and measurement of helmholts coil fields. Technical report, Army Research Laboratory, 1994.

[17] P. C. Dokko, J. A. PASK, and K. S. MAZDIYASNI. High-temperature mechanical properties of mullite under compression. *Journal of the American Ceramic Society*, 60(3-4):150–155, mar 1977. doi: 10.1111/j.1151-2916.1977.tb15492.x.

[18] H. M. Duiker, P. D. Beale, J. F. Scott, C. A. P. de Araujo, B. M. Melnick, J. D. Cuchiaro, and L. D. McMillan. Fatigue and switching in ferroelectric memories: Theory and experiment. *Journal of Applied Physics*, 68(11):5783–5791, dec 1990. doi: 10.1063/1.346948.

[19] S. Eakasit, S. Gunasekaran, and R. S. Lakes. Broadband viscoelastic spectroscopy: A new technique for characterizing rheological behavior of solid foods. *International Journal of Food Properties*, 12(1):102–113, jan 2009. doi: 10.1080/10942910802223388.

[20] J. Fischer, T. Klaassen, N. Hovenier, G. Jakob, A. Poglitsch, and O. Sternberg. Cryogenic far-infrared laser absorptivity measurements of the herschel space observatory telescope mirror coatings. *Applied Optics*, 43(19):3765, jul 2004. doi: 10.1364/ao.43.003765.

[21] D. J. Fixsen. The temperature of the cosmic microwave background. *The Astrophysical Journal*, 707(2):916, 2009. URL http://stacks.iop.org/0004-637X/707/i=2/a=916.

[22] A. J. Fleming and S. O. R. Moheimani. Adaptive piezoelectric shunt damping. *Smart Materials and Structures*, 12(1):36–48, jan 2003. doi: 10.1088/0964-1726/12/1/305.

[23] N. Fujitsuka, J. Sakata, Y. Miyachi, K. Mizuno, K. Ohtsuka, Y. Taga, and O. Tabata. Monolithic pyroelectric infrared image sensor using PVDF thin film. *Sensors and Actuators A: Physical*, 66(1-3):237–243, apr 1998. doi: 10.1016/s0924-4247(98)00050-8.

[24] P. Gao, J. Britson, J. R. Jokisaari, C. T. Nelson, S.-H. Baek, Y. Wang, C.-B. Eom, L.-Q. Chen, and X. Pan. Atomic-scale mechanisms of ferroelastic domain-wall-mediated ferroelectric switching. *Nature Communications*, 4, nov 2013. doi: 10.1038/ncomms3791.

[25] J. O. Gentner, P. Gerthsen, N. A. Schmidt, and R. E. Send. Dielectric losses in ferroelectric ceramics produced by domain-wall motion. *Journal of Applied Physics*, 49(8):4485–4489, 1978. doi: 10.1063/1.325453. URL `http://link.aip.org/link/?JAP/49/4485/1`.

[26] A. Gruverman, O. Auciello, and H. Tokumoto. Scanning force microscopy: Application to nanoscale studies of ferroelectric domains. *Integrated Ferroelectrics*, 19(1-4): 49–83, apr 1998. doi: 10.1080/10584589808012695.

[27] D. Guyomar, A. Badel, E. Lefeuvre, and C. Richard. Toward energy harvesting using active materials and conversion improvement by nonlinear processing. *IEEE Transactions on Ultrasonics, Ferroelectrics, and Frequency Control*, 52(4):584–595, April 2005. ISSN 0885-3010. doi: 10.1109/TUFFC.2005.1428041.

[28] P. G. Halverson, T. J. Parker, and M. Levine. Cryogenic performance of piezo-electric actuators for opto-mechanical applications. In W. A. Goodman and J. L. Robichaud, editors, *Optical Materials and Structures Technologies III*. SPIE-Intl Soc Optical Eng, sep 2007. doi: 10.1117/12.767306.

[29] Q. Hao, F. Hu, and Y. Xiao. Multiple human tracking and identification with wireless distributed pyroelectric sensor systems. *IEEE Systems Journal*, 3(4):428–439, dec 2009. doi: 10.1109/jsyst.2009.2035734.

[30] M. Hooker. Properties of pzt-based piezoelectric ceramics between -150 and 250 c. Technical report, Lockheed Martin Engineering and Sciences Co., Hampton, VA United States, 1998.

[31] T. Hussain, A. Baig, T. Saadawi, and S. Ahmed. Infrared pyroelectric sensor for detection of vehicular traffic using digital signal processing techniques. *IEEE Transactions on Vehicular Technology*, 44(3):683–689, 1995. doi: 10.1109/25.406637.

[32] A.-B. M. A. Ibrahim, R. Murgan, M. K. A. Rahman, and J. Osm. Morphotropic phase boundary in ferroelectric materials. In *Ferroelectrics - Physical Effects*. InTech, aug 2011. doi: 10.5772/17206.

[33] H. W. Jang, A. Kumar, S. Denev, M. D. Biegalski, P. Maksymovych, C. W. Bark, C. T. Nelson, C. M. Folkman, S. H. Baek, N. Balke, C. M. Brooks, D. A. Tenne, D. G. Schlom, L. Q. Chen, X. Q. Pan, S. V. Kalinin, V. Gopalan, and C. B. Eom. Ferroelectricity in strain-FreeSrTiO3thin films. *Physical Review Letters*, 104(19), may 2010. doi: 10.1103/physrevlett.104.197601.

[34] B. Jiménez and J. Vicente. Influence of mobile 90Â° domains on the complex elastic modulus of pzt ceramics. *Journal of Physics D: Applied Physics*, 33(12):1525, 2000. URL http://stacks.iop.org/0022-3727/33/i=12/a=315.

[35] S. Kampe, J. Schultz, A. Aning, A. Goff, and J. Franklin. Piezoelectric ceramic-reinforced metal-matrix composites, 10 2006. patent.

[36] V. G. Karnaukhov, I. F. Kirichok, and M. V. Karnaukhov. The influence of dissipative heating on active vibration damping of viscoelastic plates. *Journal of Engineering Mathematics*, 61(2-4):399–411, apr 2008. doi: 10.1007/s10665-008-9217-3.

[37] M. T. Kesim, J. Zhang, S. Trolier-McKinstry, J. V. Mantese, R. W. Whatmore, and S. P. Alpay. Pyroelectric response of lead zirconate titanate thin films on silicon: Effect of thermal stresses. *Journal of Applied Physics*, 114(20):204101, nov 2013. doi: 10.1063/1.4833555.

[38] D. Kochmann, C. Wojnar, and J. Graverend. Broadband electromechanical spectroscopy, Mar. 22 2016. URL https://www.google.com/patents/US9291536. US Patent 9,291,536.

[39] J.-B. le Graverend, C. S. Wojnar, and D. M. Kochmann. Broadband control of the viscoelasticity of ferroelectrics via domain switching. *Applied Physics Letters*, 105 (16):162912, oct 2014. doi: 10.1063/1.4899055.

[40] T. Lee, R. Lakes, and A. Lal. Resonant ultrasound spectroscopy for measurement of mechanical damping: Comparison with broadband viscoelastic spectroscopy. *Review of Scientific Instruments*, 71(7):2855, 2000. URL http://link.aip.org/link/RSINAK/v71/i7/p2855/s1&Agg=doi.

[41] J. Li, B. Nagaraj, H. Liang, W. Cao, C. H. Lee, and R. Ramesh. Ultrafast polarization switching in thin-film ferroelectrics. *Applied Physics Letters*, 84(7):1174–1176, feb 2004. doi: 10.1063/1.1644917.

[42] K. Li, J.-Y. Gauthier, and D. Guyomar. Structural vibration control by synchronized switch damping energy transfer. *Journal of Sound and Vibration*, 330(1):49–60, jan 2011. doi: 10.1016/j.jsv.2010.07.021.

[43] M. A. Lieberman and A. J. Lichtenberg. *Principles of Plasma Discharges and Materials Processing*. Wiley-Blackwell, jan 2005. doi: 10.1002/0471724254.

[44] A. J. Lovinger. Ferroelectric polymers. *Science*, 220(4602):1115–1121, jun 1983. doi: 10.1126/science.220.4602.1115.

[45] A. Lozinski, F. Wang, A. Uusimäki, and S. Leppävuori. PLZT thick films for pyroelectric sensors. *Measurement Science and Technology*, 8(1):33–37, jan 1997. doi: 10.1088/0957-0233/8/1/005.

[46] P. C. Lysne and C. M. Percival. Electric energy generation by shock compression of ferroelectric ceramics: Normal-mode response of PZT 95/5. *Journal of Applied Physics*, 46(4):1519–1525, apr 1975. doi: 10.1063/1.321803.

[47] K. Menard. Dynamic mechanical analysis. In *Encyclopedia of Polymer Science and Technology*. John Wiley & Sons, Inc., 2002. ISBN 9780471440260. doi: 10.1002/0471440264.pst102. URL http://dx.doi.org/10.1002/0471440264.pst102.

[48] W. J. Merz. Domain formation and domain wall motions in ferroelectric batio3 single crystals. *Physical Review*, 95(3):690–698, 1954. URL http://link.aps.org/doi/10.1103/PhysRev.95.690. PR.

[49] R. C. Miller and A. Savage. Motion of 180Â° domain walls in metal electroded barium titanate crystals as a function of electric field and sample thickness. *Journal of Applied Physics*, 31(4):662–669, 1960. doi: http://dx.doi.org/10.1063/1.1735663. URL http://link.aip.org/link/?JAP/31/662/1.

[50] K. M. Ok, E. O. Chi, and P. S. Halasyamani. Bulk characterization methods for non-centrosymmetric materials: second-harmonic generation, piezoelectricity, pyroelectricity, and ferroelectricity. *Chemical Society Reviews*, 35(8):710, 2006. doi: 10.1039/b511119f.

[51] D.-S. Paik, S.-E. Park, T. R. Shrout, and W. Hackenberger. Dielectric and piezoelectric properties of perovskite materials at cryogenic temperatures. *Journal of Materials Science*, 34(3):469–473, 1999. doi: 10.1023/a:1004578225228.

[52] P. Picot. La coupure du courant lectrique dans le vide. Technical report 198, Schneider Electric, 2000.

[53] X. P. Qing, S. J. Beard, A. Kumar, K. Sullivan, R. Aguilar, M. Merchant, and M. Taniguchi. The performance of a piezoelectric-sensor-based shm system under a combined cryogenic temperature and vibration environment. *Smart Materials and Structures*, 17(5):055010, 2008. URL http://stacks.iop.org/0964-1726/17/i=5/a=055010.

[54] S. Raja, P. K. Sinha, G. Prathap, and D. Dwarakanathan. Thermally induced vibration control of composite plates and shells with piezoelectric active damping. *Smart Materials and Structures*, 13(4):939–950, jun 2004. doi: 10.1088/0964-1726/13/4/032.

[55] D. J. Santeler. *Vacuum technology and space simulation*. Scientific and Technical Information Division, National Aeronautics and Space Administration, 1966.

[56] S. Saremi, R. Xu, L. R. Dedon, J. A. Mundy, S.-L. Hsu, Z. Chen, A. R. Damodaran, S. P. Chapman, J. T. Evans, and L. W. Martin. Enhanced electrical resistivity and properties via ion bombardment of ferroelectric thin films. *Advanced Materials*, 28 (48):10750–10756, oct 2016. doi: 10.1002/adma.201603968.

[57] A. Savage and R. C. Miller. Temperature dependence of the velocity of sidewise 180Â° domain-wall motion in batio$_3$. *Journal of Applied Physics*, 31(9):1546–1549, 1960. doi: http://dx.doi.org/10.1063/1.1735890. URL http://link.aip.org/link/?JAP/31/1546/1.

[58] C. B. Sawyer and C. H. Tower. Rochelle salt as a dielectric. *Phys. Rev.*, 35:269–273, Feb 1930. doi: 10.1103/PhysRev.35.269. URL http://link.aps.org/doi/10.1103/PhysRev.35.269.

[59] N. A. Schmidt. Coercive force and 90Â° domain wall motion in ferroelectric plzt ceramics with square hysteresis loops. *Ferroelectrics*, 31(1):105–111, 1981. ISSN 0015-0193. doi: 10.1080/00150198108201980. URL http://www.tandfonline.com/doi/abs/10.1080/00150198108201980.

[60] R. E. Setchell. Shock wave compression of the ferroelectric ceramic pb0.99(zr0.95ti0.05)0.98nb0.02o3: Hugoniot states and constitutive mechanical properties. *Journal of Applied Physics*, 94(1):573–588, jul 2003. doi: 10.1063/1.1578526.

[61] I. Shibuya and S. Hoshino. Re-examination of the thermal expansion of the ferroelectric triglycine sulfate. *Japanese Journal of Applied Physics*, 1(5):249, 1962. URL http://stacks.iop.org/1347-4065/1/i=5/a=249.

[62] D. Sinha. Acoustic resonance spectroscopy (ARS). *IEEE Potentials*, 11(2):10–13, apr 1992. doi: 10.1109/45.127718.

[63] V. Skoromets, C. Kadlec, H. Nemec, and P. Kuzel. Terahertz dielectric properties of $KTaO_3$ crystal: Electric-field tunability, comparison with $SrTiO_3$. In *2016 41st International Conference on Infrared, Millimeter, and Terahertz waves (IRMMW-THz)*. Institute of Electrical and Electronics Engineers (IEEE), sep 2016. doi: 10.1109/irmmw-thz.2016.7758799.

[64] G. Srivastava, M. Maglione, and A. M. Umarji. The study of dielectric, pyroelectric and piezoelectric properties on hot pressed PZT-PMN systems. *AIP Advances*, 2(4): 042170, dec 2012. doi: 10.1063/1.4769889.

[65] A. K. Tagantsev, I. Stolichnov, E. L. Colla, and N. Setter. Polarization fatigue in ferroelectric films: Basic experimental findings, phenomenological scenarios, and microscopic features. *Journal of Applied Physics*, 90(3):1387–1402, aug 2001. doi: 10.1063/1.1381542.

[66] R. P. Taylor. Measurements of the material properties of a laminated piezoelectric stack at cryogenic temperatures. In *AIP Conference Proceedings*. AIP Publishing, 2006. doi: 10.1063/1.2192352.

[67] D. A. Tenne, A. Soukiassian, X. X. Xi, T. R. Taylor, P. J. Hansen, J. S. Speck, and R. A. York. Effect of thermal strain on the ferroelectric phase transition in polycrystalline ba0.5sr0.5tio3 thin films studied by raman spectroscopy. *Applied Physics Letters*, 85 (18):4124–4126, nov 2004. doi: 10.1063/1.1813625.

[68] W. Thompson. *On the thermoelastic, thermomagnetic and pyroelectric properties of matter*, volume 5 of *5*, pages 4–26. Philosophical Magazine, 1878.

[69] C. F. Tsai and M. S. Young. Pyroelectric infrared sensor-based thermometer for monitoring indoor objects. *Review of Scientific Instruments*, 74(12):5267–5273, dec 2003. doi: 10.1063/1.1626005.

[70] T. Tsurumi, S. M. Nam, Y. B. Kil, and S. Wada. Frequency dependence of p-e hysteresis curves in PZT thin films. *Key Engineering Materials*, 214-215:123–128, 2002. doi: 10.4028/www.scientific.net/kem.214-215.123.

[71] J. Valasek. Piezo-electric and allied phenomena in rochelle salt. *Physical Review*, 17 (4):475–481, apr 1921. doi: 10.1103/physrev.17.475.

[72] K. Visvanathan and Y. B. Gianchandani. Ultrasonic microheaters using piezo-ceramics for cauterization and other applications. In *TRANSDUCERS 2009 - 2009 International Solid-State Sensors, Actuators and Microsystems Conference*. Institute of Electrical and Electronics Engineers (IEEE), jun 2009. doi: 10.1109/sensor.2009.5285433.

[73] C. Wojnar and D. Kochmann. A negative-stiffness phase in elastic composites can produce stable extreme effective dynamic but not static stiffness. *Philosophical Magazine*, 2013. under review.

[74] C. S. Wojnar. *Exploring the Kinetics of Domain Switching in Ferroelectrics for Structural Applications*. PhD thesis, California Institute of Technology, 2015.

[75] C. S. Wojnar, J.-B. le Graverend, and D. M. Kochmann. Broadband electromechanical spectroscopy: A method for measuring the dynamic electromechanical response of ferroelectrics. In *Micro and Nanomechanics, Volume 5*, pages 63–71. Springer Nature, sep 2016. doi: 10.1007/978-3-319-42228-2_10.

[76] C. Wong, O. Diehm, and D. Van Aken. Damping capacity of aluminum 6061-indium alloys. Technical report, DTIC Document, 1990.

[77] P. Wurfel and I. P. Batra. Depolarization-field-induced instability in thin ferroelectric films—experiment and theory. *Physical Review B*, 8(11):5126–5133, dec 1973. doi: 10.1103/physrevb.8.5126.

[78] X. Xia, Y. Wang, Z. Zhong, and G. J. Weng. Theory of electric creep and electromechanical coupling with domain evolution for non-poled and fully poled ferroelectric ceramics. *Proceedings of the Royal Society A: Mathematical, Physical and Engineering Science*, 472(2194):20160468, oct 2016. doi: 10.1098/rspa.2016.0468.

[79] F. Xu, S. Trolier-McKinstry, W. Ren, B. Xu, Z.-L. Xie, and K. J. Hemker. Domain wall motion and its contribution to the dielectric and piezoelectric properties of lead zirconate titanate films. *Journal of Applied Physics*, 89(2):1336–1348, jan 2001. doi: 10.1063/1.1325005.

[80] B. Yurke, P. Kaminsky, and D. Eigler. Cryogenic piezoelectric displacement tester. *Cryogenics*, 26(7):435–436, jul 1986. doi: 10.1016/0011-2275(86)90091-3.

[81] J. Zhang, R. J. Perez, and E. J. Lavernia. Documentation of damping capacity of metallic, ceramic and metal-matrix composite materials. *Journal of Materials Science*, 28(9):2395–2404, 1993. doi: 10.1007/bf01151671.

[82] J. X. Zhang, P. C. W. Fung, and W. G. Zeng. Dissipation function of the first-order phase transformation in solids via internal-friction measurements. *Physical Review B*, 52(1):268–277, jul 1995. doi: 10.1103/physrevb.52.268.

[83] T.-Y. Zhang, M. Zhao, and P. Tong. Fracture of piezoelectric ceramics. In *Advances in Applied Mechanics*, pages 147–289. Elsevier BV, 2002. doi: 10.1016/s0065-2156(02)80104-1.

[84] D. Zhou, M. Kamlah, and D. Munz. Rate dependence of soft pzt ceramics under electric field loading. *Proc. SPIE*, pages 64–70, 2001. doi: 10.1117/12.432740. URL `http://dx.doi.org/10.1117/12.432740`. 10.1117/12.432740.

[85] T. Zhu, F. Fang, and W. Yang. Fatigue crack growth in ferroelectric ceramics below the coercive field. *Journal of Materials Science Letters*, 18(13):1025–1027, 1999. doi: 10.1023/a:1006663108103.

VITA

William Kent Hays Was born in Richmond, Virginia, February 14^{th}, 1993. He received his Bachelors of Science in Engineering from James Madison University in May 2015. During the course of his education at JMU he was involved with several research projects, two of which have been published in ASME Early Careers Technical Conference (*Energy Usage Modeling and Measurements for an Electric Motorcycle on a Cross Country Route*, University of Alabama Birmingham, November 2–3, 2013) and also by IEEE Systems and Information Engineering Design Symposium (*Electric Commuter Bicycle*, University of Virginia, 2015). In July, 2017, he received his Masters of Science degree in Mechanical Engineering from Missouri University of Science and Technology.